MECHANICAL AND RHEOLOGICAL CHARACTERIZATION OF THE CORNEA

By

EBITIMITULA ETEBU

Bachelor of Science in Mechanical and Aerospace Engineering

Oklahoma State University

Stillwater, Ok

2010

Submitted to the Faculty of the
Graduate College of the
Oklahoma State University
in partial fulfillment of
the requirements for
the Degree of
MASTER OF SCIENCE
December, 2013

MECHANICAL AND RHEOLOGICAL

CHARACTERIZATION OF THE CORNEA

Thesis Approved:

Dr. Hamed Hatami-Marbini

Thesis Adviser

Dr. James Good

Dr. Wei Yin

ACKNOWLEDGEMENTS

I thank GOD for giving me the strength, courage and ability to complete my masters. I would like to thank Dr. Hamed Hatami-Marbini for his advice, guidance and patience throughout the duration taken to complete this work. I would also like to thank Dr. James Keith Good and Dr. Wei Yin for being my committee members and providing valuable suggesting throughout my thesis, Dr. Sundar V. Madihally for letting us use his facilities, as well as fruitful discussions towards the preliminary work done to characterize GAG depleted corneas.

I am very grateful to family; Dr. E.N. Etebu, Dr. O.M. Etebu, Jessica Smith, Fiona Etebu, Stephanie Etebu, and Brooke Etebu for their love support and encouragement through this process. I would also like to acknowledge my colleagues that helped and motivated me from the class room to the research environment.

Acknowledgements reflect the views of the author and are not endorsed by committee members or Oklahoma State University.

Name: EBITIMITULA ETEBU

Date of Degree: December, 2013

Title of Study: MECHANICAL AND RHEOLOGICAL CHARACTERIZATION OF THE CORNEA.
Major Field: Mechanical Engineering

Abstract: The cornea is a semi-permeable connective tissue with multiple simultaneous functions that include load bearing, hydration regulation via fluid transport, maintaining eye ball shape, and transmitting incident light without scattering. Cornea is the transparent outer coat of the eyeball that provides 70% of the eyes refractive power. It is also a load bearing material that protects the inner ocular contents from accidental impacts. From a mechanical standpoint, the cornea is a semipermeable hydrophilic gel with a fibrillar components and negatively charged proteoglycans. The cornea's capability to transmit light is dependent on its ability to maintain its unique structure, which gives rise to its mechanical properties. In this thesis, mechanical properties of the corneal stroma were characterized. Unconfined compression was used to characterize compressive properties of the porcine corneal stroma. Using this technique, this research study characterized the effects of environmental parameters, e.g temperature, sample thickness and diameter. Furthermore, a rheometer was used to conduct the torsional shear experiments and measure shear properties of the tissue.

It was observed that the cornea displayed time dependent behavior. The theoretical biphasic model was used to numerically represent the transient compressive behavior observed in experimental measurements and predict the material parameters of the cornea. The in-plane Young's modulus, out-of plane Young's modulus, and permeability of the porcine cornea were estimated as a function of tissue thickness and loading rate. In the end, a finite element biphasic model of the corneal behavior in construction was constructed. The results of the finite element analysis was mesh size dependent but converged to the theoretic and experimental measurements using very fine mesh.

In summary, this thesis characterized compressive and torsional mechanics of the porcine cornea at varying compressive strains. It is expected that the findings of the present work would enhance the accuracy of corneal constitutive models, these numerical models are necessary for calibrating applanation tonometry devices which are commonly used in clinical measurements. In addition, the reported data in this thesis can be used to compare the mechanical properties of engineered corneal equivalents with those of the native tissue.

TABLE OF CONTENTS

Chapter Page

Chapter Page

LIST OF TABLES

LIST OF FIGURES

Figure Page

Figure Page

Figure Page

Figure Page

SYMBOLS AND ABBREVIATION

IOP……....Intraocular pressure

IS…….Inferior-superior

NT……..Nasal-temporal

WAXRD……Wide angle xray-diffraction

GAG …….Glycosaminoglycan

SP……...Swelling pressure

$\Delta\pi$……...……Osmotic pressure

P_t……Tissue pressure

C_f ……..…Concentration of stromal fixed charge

Na_0……Concentration of the sodium ions

V_s…….…….Stromal volume

Γ ……Helmholtz free energy

σ_{ch}…….Chemical stresses

P_{fl}……Fluid pressure

$H_A(c)$ ……..Confined compressive modulus

OBSS..…….Ophthalmic balanced salt solution

T……..Torque

R……Radius of parallel plate

θ……..Angular displacement

H_i…….height of sample

τ …….…….Shear stress

γ ……..shear strain

ω……Frequency

T_0……...Torque amplitude

δ……...Phase shift angle

G'……Storage modulus

G" ……...…….Loss modulus

G(t) ……...……Stress relaxation modulus

LVL……..…Linear viscoelastic limit

τ_1……...Short term time

τ_2 ……...Long term time

C……Dimensionless spectrum magnitude

$\boldsymbol{\sigma}^{SM}$ ……..Solid matrix stress

$\boldsymbol{\sigma}^{E}$ ……..Elastic stress tensor

P……Pressure

ϕ^{s} ……Solid volume fraction

ϕ^{f} ……....Fluid volume fraction

$\boldsymbol{\sigma}^{F}$ …..……..Fluid Stress

$\mathbf{I}$……..Identity Matrix

$\boldsymbol{C}_{ij}$……Fourth Order stiffness tensor

$\boldsymbol{E}_{r}$……In-plane Young's modulus

$\upsilon_{r\theta} = \upsilon_{\theta r}$…….In-plane Poisson's ratio

$\boldsymbol{E}_{z}$……Out of plane Young's modulus

$\boldsymbol{G}_{zr}$……..Shear modulus

∇……Del operator

$\boldsymbol{V}^{s}$……Solid phase velocity

$\boldsymbol{V}^f$…….Fluid phase velocity

κ_r……..Radial permeability

u_r……...……..Radial displacement in cylindrical coordinates

$\epsilon(t)$……...……..Experimentally applied strain

ε_{ij}……...Elastic strain matrix

$J_{1,0}$……..Bessel functions of the first kind

CHAPTER I

INTRODUCTION

1.1 Motivation

The eye is a complex optical organ that is comprised of three layers namely the outer, middle, and inner coat where each coat contributes to our vision[2]. The outer coat is comprised of an opaque sclera and a transparent cornea; these structural tissues are responsible for the protection of internal ocular contents and shaping the eye globe[3]. Uvea is the eyes middle coat, it regulates light entering the eye, alter refractive power, in addition to absorbing light and nutrition. Retina (inner coat) is a sensory tissue in the back of the eye that transmits light through the optic nerve to the brain, thus generating vision.

Light entering the eye is refracted at the anterior and posterior surfaces of the cornea and lens before it reaches the retina. The cornea is responsible for about 70% of the eyes refractive power[4], thus it can be considered as the primary refractive element of the eye. Corneal disease is the secondary leading cause of blindness globally[5] of which corneal opacity is responsible for 5.1% of all global blindness thus the characterization of corneal behavior has generated high level of interest[6-13]. Refractive power of the cornea is governed by its anterior and posterior curvature while corneal transparency is governed by its complex ultrastructure. Corneal refractive defects caused by shape change or loss of rigidity as observed in astigmatism, myopia and keratoconus disease results in altered vision and blindness.

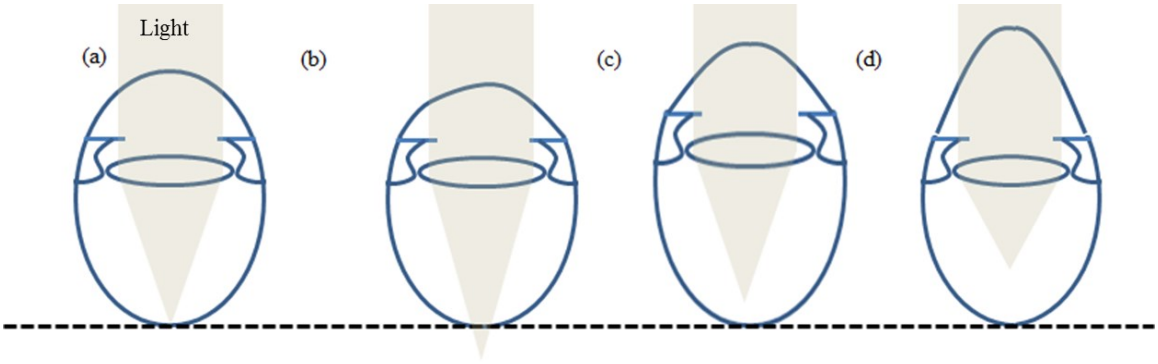

Figure 1.1: Schematic of focused light in (a) healthy cornea (b) astigmatism (c) myopic corneas (d) cone shaped cornea. Dotted line represents retina where refracted light should be focused.

Refractive surgical techniques employ alteration of the corneal surface curvature or cross-linking to correct refractive errors and corneal rigidity. Photorefractive keratectomy (PRK) and Laser assisted sub-epithelial keratectomy (LASEK) are refractive surgical techniques that implements photoablation via an excimer laser to alter the anterior surface of the cornea by the removal of some anterior corneal stromal tissue[14-16]. When corneal defects are beyond correction by refractive surgery, corneal transplantation provides a therapeutic solution for opacification or corneal blindness. Corneal transplantation is the most successful tissue transplantation for humans where success rate of up to 90% has been reported. Nevertheless, this procedure is limited to the availability of healthy donor tissues as only approximately 100,000 corneas are collected by eye banks worldwide which are diminutive in comparison to the 4.5 million individuals suffering from blindness due to corneal scaring. A solution proposed to the lack of healthy donor cornea is the use of tissue engineered corneas for transplant[17, 18].

In order to advance the current therapeutic options for corneal defects, a better understanding of the cornea's mechanical properties is essential to attain the predictive response of refractive a surgery, as well as a control for developing engineered corneal equivalents[17, 18]. For instance, the ability to predict the alteration of corneal curvature as used in refractive surgery is dependent on

corneal mechanical behavior, where corneal mechanical behavior can be characterized experimentally. Using constitutive models to evaluate the experimentally attained behavior, the cornea's deformation can be predicted under varying loading conditions thus providing the refractive surgeon with a possible outcome of the change in shape of the cornea.

1.2 Aim of study

The aim of the research work in this thesis includes;

(a) Experimental characterization of the static and time dependent mechanical properties of the cornea and the effect of loading rate on instantaneous and transient mechanics.

(b) Theoretical analysis of the experimentally observed behavior in order to fully characterize the elastic tensile modulus and permeability at varying swelling pressures/thicknesses.

1.3 Approach

Mechanical properties of porcine corneas were investigated using the unconfined compression testing technique. This method was implemented to characterize the static, time dependent and rate dependent behavior of the corneal stroma. A transversely isotropic biphasic model was curve fitted to the experimental results attained in order to determine the mechanical parameters of the corneal stroma. Corneal shear mechanics were also investigated by applying static and dynamic oscillatory shear loads.

CHAPTER II

LITERATURE REVIEW

2.1 Function and structure of the cornea

The cornea is a semi-permeable connective tissue with multiple simultaneous functions that include load bearing, hydration regulation via fluid transport, maintaining the eye ball shape, and transmitting incident light without scattering. The nature of *in vivo* loads applied to the cornea dictates it is always under tensile loads from intraocular pressure[19] and connection at corneoscleral junction. Compressive and shear loads are also applied to the cornea from applanation of eye lids, clinical devices, surgical device, eye rubbing or accidental projectiles. The cornea possesses a conical geometry[20] where the nasal-temporal (NT; horizontal) diameter is generally larger than the inferior-superior (IS; vertical) diameter[21-23] (Figure 2.1). Thickness of the cornea is also observed to be thinner in the central region in comparison to the peripheral region[22, 24] as seen in human and porcine corneas, however corneas from animal species such as rabbit and bovine have been observed to display uniform diameter[25, 26]. Ocular dimensions of corneas commonly used in mechanical studies are given in Table 2.1. based on reports of previous studies[21-23, 26-28]. The cornea is generally composed of epithelium, Bowman's layer, stroma, Descemet's membrane and endothelium from its anterior to posterior[3, 9, 29-32]; an extensive study of the Bowman's layer by Merindano et al. (2002) [33] observed the Bowman's layer is absent in carnivores, and some herbivores such as equine and porcine.

The epithelium is a stratified squamous anterior membrane composed of up to three distinct cells where its anterior cells are flattened squamous cells, wing cells encompass the middle region, and the posterior region is composed of basal cells[34]. The epithelial layer is responsible for about 10% of the corneal thickness in humans[35, 36] and ~9% in porcine[22]. The epithelium is composed of 75%[14] equivalent water content. It is responsible for the absorption of nutrients and oxygen from the tear film[37], regulation of fluid transport through the cornea, and it protects the stroma from disease[38]. Contribution of the epithelium to corneal mechanics has been reported to be minimal in comparison to other components of the cornea[35, 39, 40].

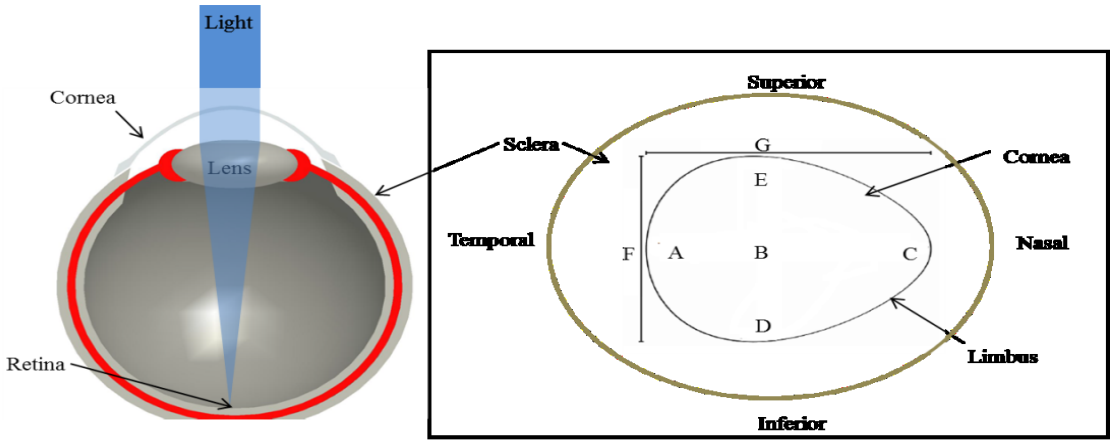

Figure 2.1: (Left) Schematic of the eye globes cross section showing the refraction of light through the cornea and lens before transmission to the sclera. (Right) Front view of the eyes outer coat displaying symbols for the ocular dimensions of the cornea used in table 2.1

Table 2.1: Reported corneal dimensions for various species used in mechanical characterization.

	A mm	B mm	C mm	D mm	E mm	F mm	G Mm	Curvature mm	Reference #
Human	0.565	0.540	0.566	0.559	0.579	10.5	11.8	7.7-7.8	9,14,13
Porcine	0.669	0.666	0.657	0.713	0.714	12.4	14.9	8.45	7,8
Rabbit	0.412	0.407	0.403	0.393	0.406	13.1	13.4	7.1-7.3	12,13

Below the epithelium is a relatively thin Bowman's layer, it is one of the corneal layers that contain collagen fibrils. These collagen fibrils are randomly arranged and their diameters have been measured to be within 20-30 nm in human corneas[32, 41]. Collagens of types I, III, IV, V, VI are reported to be present in the Bowman's membrane[42-45]. The stroma is responsible for about 90% of the corneas thickness; it is has been reported to dominate the tensile load bearing[30, 35, 40], fluid imbibition and swelling[31, 46-48] characteristics of the cornea.

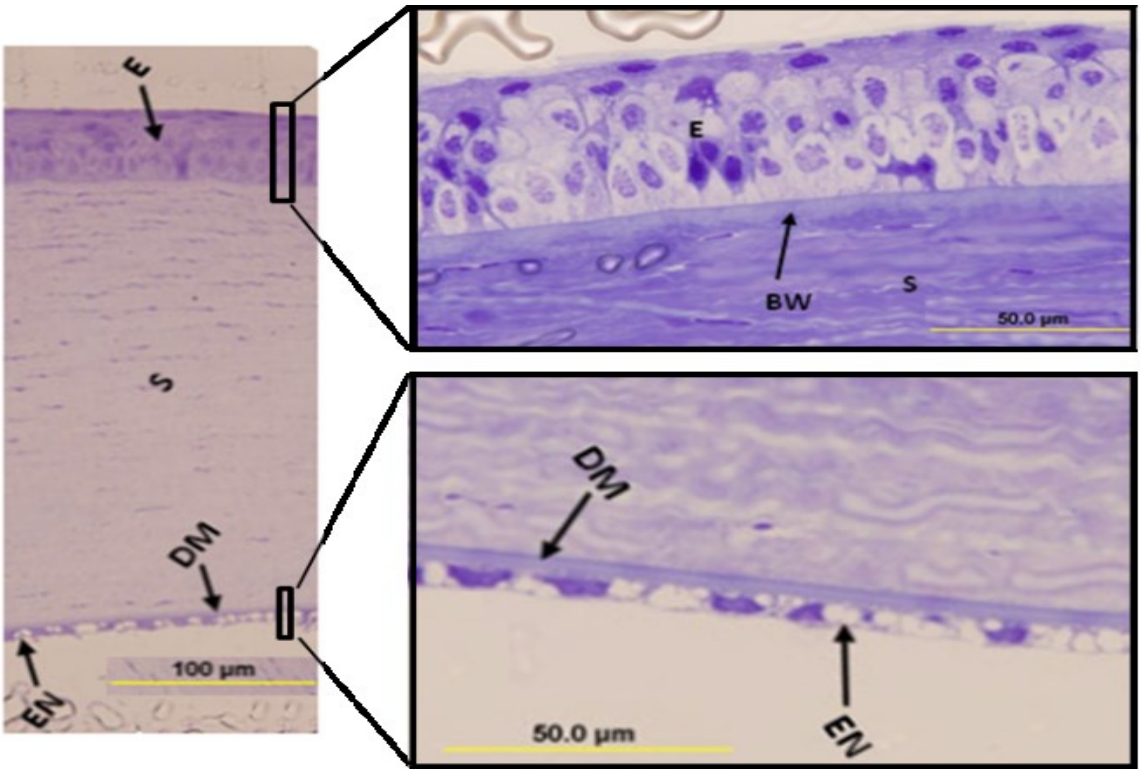

Figure 2.2: Light micrograph of the through thickness corneal cross-section of the cornea displaying the epithelium (E), Bowman's membrane (BW), stroma (S), Descemet's membrane (DM) and endothelium (EN) (with permission from [49]).

The Descemet's membrane is a basement membrane that provides support to endothelial cells[39], it is a laminated structure composed of type II, IV, VI and VII collagen as well as non-collagenous glycoproteins[42, 50-52]. Previous studies characterizing isolated Descemet's membrane reported its contribution to load bearing capabilities of the cornea[39, 40] where it was observed that

its contribution to bearing tensile loads is minimal. The endothelium is the delicate posterior layer of the cornea composed of a single layer of about 400,000 hexagonal endothelial cells[53, 54], it functions as a fluid transport barrier for nutrition and ion fluid pump that regulates the *in vivo* hydration of the cornea[55].

2.2 Architecture of the corneal stroma

The stroma is a hydrated matrix composed of collagen, proteoglycans, keratocytes, salts, and glycoproteins. At physiological state, the average equivalent water content of the stroma is reported to be about 75-83%[14, 56, 57] for various species which results in a tissue hydration in the range of 3.2-3.45 mg H_20/mg dry tissue[7, 58, 59]. Furthermore collagen, proteoglycans, and keratocytes are reported to account for 15-16%[34], 1%[34], 2-5%[37, 60, 61] of the stromal content at physiological hydration. In dried state, collagen, keratocytes and proteoglycans are reported to be responsible for 68%, 10%, and 9% of the stromal dry weight respectively[62].

2.2.1 Collagen

Transparency of the stroma and its ability to transmit about 99% of incident light without scattering arises from the arrangement of collagen fibrils[63]. It is also responsible for the tensile response of the cornea[64-66]. Stromal collagens are reportedly composed of heterotypic collagen fibrils rich in type I collagen (58%), type III (10%) and type V collagen (5%) of the collagen dry weight respectively; the distribution of type I and V fibrils within the same fibril is reported to regulate collagen fibril diameter[67]. Type III collagen content is reported to increase during inflammation and in the process of wound healing. Additional collagens of type VI, IX, XII, XIII, and XIV are reported to be present in the cornea; where collagen type VI generate micro fibrillar structures, and type XIII are non fibrillar collagen that attach to cell membranes. Type XIV and

XII are fibrils associated collagens with interrupted triple helices[68-70] that are vital in the regulation collagen fibrils function and structure[71]. Collagen fibrils in the cornea possess a uniform dimension and orientation with uniform fibril diameters, regular interfibrillar spacing, where fibrils are stacked parallel to one another in a quasi-regular hexagonal packing arrangement that forms a lamellae. There are several hundreds of lamellae in the stroma; through the corneal thickness, lamellae lay mostly in parallel arrangements in the posterior stroma while the lamellae in the anterior stroma region display interweaving. Fibril diameter and interfibrillar spacing are reported to vary between species; in human cornea, collagen fibril diameters are 30.8±0.8 nm, with an interfibrillar spacing of 55.3±4.0 nm and a lamellae thickness of 0.2-2.5 μm, width of 10-320μm with about 250-300 lamellae through the corneal depth[63]. Species such as porcine, rabbit, and bovine commonly used in experimental studies are reported to possesses collagen fibrils of average diameters within the range of 36.9-38.8 nm, and interfibrillar spacing in the range of 56.8-65.6 nm[63, 72]. Arrangement of the lamellae in the planar direction is reported to vary across species where x-ray scattering studies have reported isotropic and anisotropic lamellae orientations. A comprehensive study by Hayes et al.[73] reported the variation of x ray scatter intensity of various mammalian corneas over 360 degree angle of orientation starting at the nasal position in a counter clockwise manner using wide angle x-ray diffraction (WAXRD). Intensity and alignment of the scatter indicates that most of the collagen fibrils in human cornea are oriented in the IS direction as well as the NT direction in the central region while the peripheral region displays a circumferential preferential orientation of collagen. Advancement in characterization of three dimension orientation of collagen displayed variation of collagen preferential orientation through corneal thickness where human corneas were cut in three planar pieces from anterior to posterior. The anterior, middle and posterior sections of the cornea were observed to display varying preferential orientations where; no consistent preferential direction was observed in the anterior section, orthogonal preferential directions of collagen was observed

in the middle and posterior regions. Furthermore, preferential arrangement of posterior section was similar to the arrangement observed in full corneas.

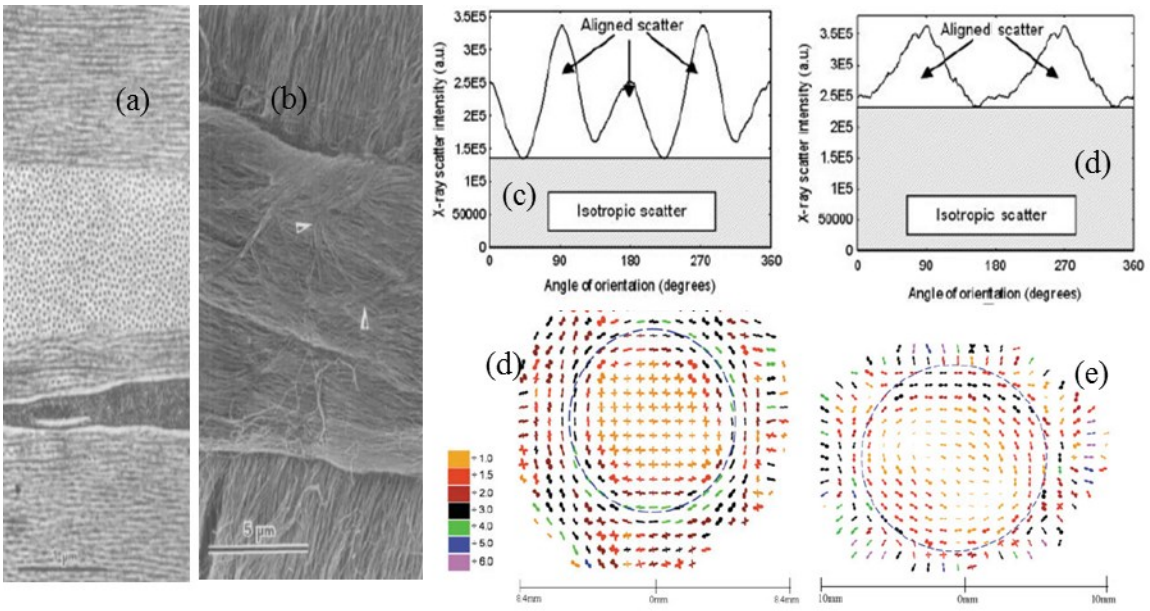

Figure 2.3: High magnification transmission electron micrographs of (a) through thickness cross sectional view of the collagen lamallae (b) planar view of lamellae with varying collagen fibril arrangement[32]. X-ray scatter intensity attained from WAXRD for (c) human cornea (d) porcine cornea[73]. Vector plot interpretation of collagen orientation in (d) human cornea (e) porcine cornea.(with permission taken from[73])

Table 2.2: Collagen fibril diameter, spacing and orientation for species commonly used in corneal studies. Symbol "+" indicate preferential orientation in the NT and IS direction, "I" for IS direction and "0" circumferential direction. Multiple symbols indicate the transition from initial preferential orientation in the central region to a secondary preferential orientation in the peripheral region.

	Fibril diameter (nm)	Inter fibrillar spacing (nm)	Intermolecular spacing (nm)	Orientation	Reference #
Human	30.8±0.8	55.3±4	1.63	"+" and" 0"	63, 73
Bovine	38.2	56.8±4.5	1.6	"I" and "0"	63, 73
Porcine	36.9±3.2	58.6±4.5	1.57±0.01	"0"	63, 73
Rabbit	38.8	58.8±4.5	1.58±0.06	"0"	63, 73

2.2.2 Proteoglycans

Proteoglycans are reported to dominate the fluid imbibition behavior of the corneal stroma[74] which might control interfibrillar spacing of collagen[75, 76] required for transparency. Alteration of proteoglycan synthesis due to disease or wound healing has been reported to muddle stromal collagen fibril arrangement[69, 70]. Proteoglycans are composed of a core protein molecule that are covalently linked with side chains of repeating disaccharide units known as glycosaminoglycan (GAG) [36]. There are four types of GAGs that are reported to be present in the cornea where keratan sulfate, dermatan sulfate, and chondroitin sulfate are responsible for most of the GAG content in addition to minor quantities of heparin sulfate[67, 77]. Keratan sulfate is mostly located in the posterior stroma where it is linked to lumican, keratocan, and mimecan core proteoglycans with atomic weights of 38 kDa, 38 kDa, and 35 kDa respectively[68]. The sulphation of these proteoglycans results in the hydrophilic swelling behavior of the stroma. Also, lumican has been shown to regulate the thickness and organization of collagen fibrils[78].

Chondroitin sulfate and dermatan sulfate are linked to decorin core proteoglycans with an atomic weight of 40 kDa[68, 79]. These proteoglycans are more abundant in the anterior portion of the cornea where the ratio of keratan sulfate to chondroitin sulfate is about 1.6 at the anterior and 2.23 at the posterior[34]. This occurrence is reported to be due their strong water retention capabilities which are essential at the anterior stroma due to higher levels of evaporation as it is closer to the external environment. A detailed study by Scott and Bosworth (1990)[80] quantified the amount of proteoglycans in various primates using light microscopy, Cupromeronic Blue, Alcain Blue staining, as well as chondroitinase ABC, and keratanase enzyme digestion. Their reports indicate that keratan sulfate is responsible for about 50% of the total GAGs content while the most of the remaining GAGs are from the ratio of chondroitin/dermatan sulfate. Average chondroitin sulfate content is reported as 200±25 (mg/g of hydroxyproline) where the mean from

various species were within 13% of this value. Dermatan sulfate was reported to amount for 20-30% of the ratio of chondroitin/dermatan sulfate. Increase in keratan sulfate and decrease in dermatan sulfate in various species were reported to coincide with an increase in species corneal thickness. Furthermore the percent of keratan sulfate content is greater in porcine (~50%) and bovine (~50%) corneas in comparison to rat corneas (~20%).

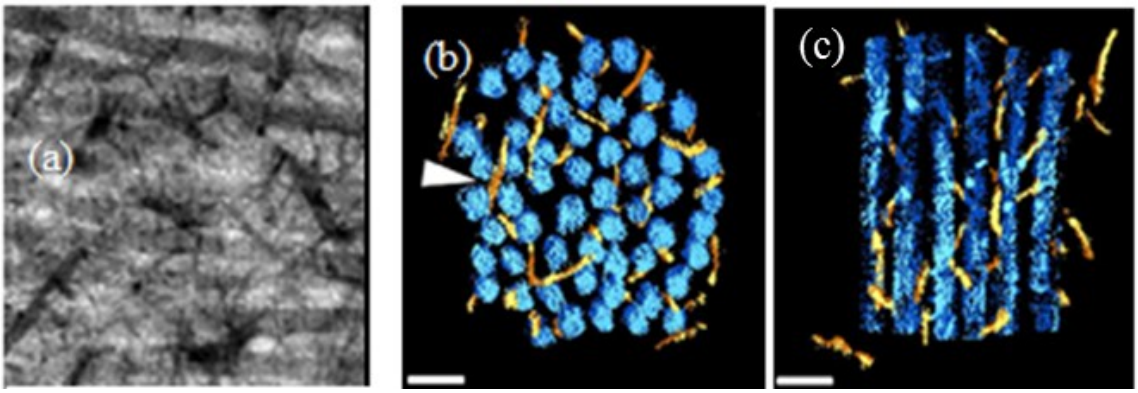

Figure 2.4: (a) Light micrographs of the corneal stroma displaying proteoglycans and glycosaminoglycan. (b) Reconstruction of collagen and proteoglycans in the corneal stroma (c) reconstruction shown through collagen length. White scale bars indicate 50 nm. (with permission from[81])

2.3.3 Keratocytes

Keratocytes are stellate stromal cells that produced proteoglycans and collagen in the stroma; they are also responsible for maintaining the stromal extracellular matrix homeostasis.[34, 82] These stellate cells are reported to occur between collagen lamellar. Keratocytes cells are quiescent except in the occurrence of injury where keratocytes undergo apoptosis or shift to repair phenotypes for wound healing.[83]

Keratocyte apoptosis is reported to be a nonthreatening response as the death of keratocytes to prevent additional loss of transparency and swelling, moreover it is reported that dead keratocytes are replaced by new keratocytes via proliferation and mitosis[83, 84]. Phenotype keratocytes are reported to drift to the site of injury where they restock the stroma by producing collagen[82].

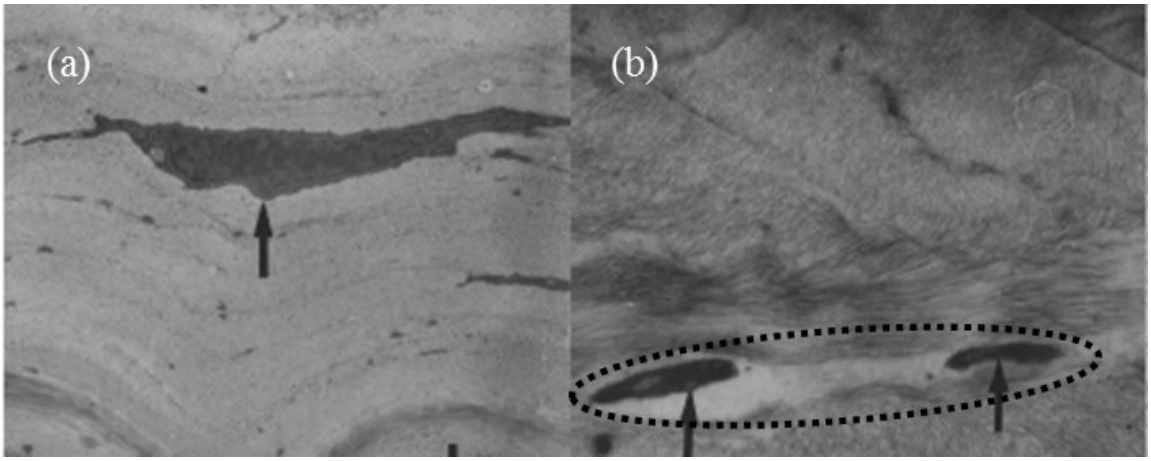

Figure 2.5: TEM micrographs (25,000 x) of mouse corneas where arrows indicate (a) Normal keratocytes in unwounded cornea (b) keratocytes observed an hour post epithelial injury where apoptosis is observed based on the fragments of keratocytes remaining (with permission from[83]).

2.3 Corneal mechanical testing

The earliest form of mechanical characterization of corneal behavior was based on characterizing pressure required to maintain the cornea at a constant thickness/hydration. Kinsey and Cogan (1942)[6] reported mechanical swelling pressure (SP) tests in cat corneas, this method was later modified Hedbys and Dohlman in 1962[85]. Tensile mechanical properties of the cornea were also studied by Nyquist in 1968 where uniaxial tension was applied to study corneal mechanics[10]. Biaxial tension was employed by Woo and Kobayashi in 1972 where fluid or air pressurization was used to conduct tensile tests on the cornea[86]. Less common characterization techniques such as indentation and compression have also been employed to characterize corneal mechanics, however the use of these techniques are shown to be promising in characterizing corneal mechanics at varying degrees of deturgescence and its the local mechanics.

2.3.1 Swelling pressure and compression

Swelling pressure is the pressure required to maintain a constant corneal thickness. Kinsey and Cogan (1942) performed swelling pressure experiments on pieces of excised cat corneas where the excised corneas were placed in a porous aluminum disc inside a hollow brass cylinder after which brass weights were placed on the cornea and immersed in fluid. When 1% NaCl was used as the immersion fluid, a pressure of about 30 mmHg was required to keep the corneal thickness constant. Hedbys and Dohlman (1962)[46, 85] implemented the use of a manometer and a transducer connected to thin aluminum rod attached to a glass filter disc to apply force on circular corneal stromas confined within a brass ring. The brass ring was sealed with a glass filter disc at the bottom in a submersion dish where 0.9% NaCl was used as the immersion fluid. Applied force was recorded by a transducer until the recorded force was steady after which corneal stroma was removed from the device and weighed; this procedure was repeated multiple times to attain the variation of SP at different hydrations of the corneal stroma. A swelling pressure of approximately 60 mmHg was reported for bovine, rabbit and human corneas at a hydration of 3.4 mg H_20/mg dry wt. Ytterborg and Dohlman (1965) utilized the method of and Hedbys and Dohlman[9] to study a larger sample of human corneas where a SP of about 50 mmHg was attained at hydration of 3.4 mg H_20/mg dry wt. The SP of dogfish corneas were studied by Toplin et al. (1965)[87] where modifications was made to the method used to determine hydration by Hedbys and Dohlman; instead of the continuous removal of the corneal stroma after force equilibrium to determine its current hydration, hydration was expressed as a function of the displaced volume and density of the displaced fluid in and the weight fraction of salt in the immersing solution. Friedman et al. (1972)[88] studied the effect of ionic concentration on rabbit corneal stromas where it was concluded from their experimental results that Donnan effect is not solely responsible for corneal stromal swelling as negative electrostatic contributions from GAG chains, excluded volume effect from the free energy of mixing, and short range polymer-solvent interactions[89]; a

SP of about 60 mmHg was reported at hydrations of approximately 3 mg H_20/mg dry wt. when immersed in 0.9% NaCl. Fatt (1971)[90] studied the coefficient of thermal expansion of rabbit corneal stromas at a constant SP where circular corneal stromas were compressed between two porous stainless steel platens in the absence of radial confinement. Sample thickness at constant SP of 53 mmHg for tests when temperature was changed from 1°C to 37°C or 37°C to 10°C were used to calculate the coefficient of thermal expansion where coefficient of thermal expansion of $-1.7\times10^{-3°C}$ and $-1.9\times10^{-3°C}$ were attained respectively. This technique was also applied by Wiley and Fatt (1975)[91] to determine the effect of varying salt solutes at varying pH on the SP of rabbit corneal stroma. Hodson et al. (1981)[92] also studied the SP of human corneas at hydration levels lower than physiological hydration in 0.9% NaCl; corneal stromas were compressed between a rigid ram and a Perspex beam connected to a strain gauge, and no radial confinement was applied to corneal stroma. Swelling properties of anterior and posterior stroma were studied by Lee and Wilson (1981)[47] where it was observed that at a constant SP the anterior stroma was more hydrated than the posterior stroma. Using human corneal stromas, Olsen and Sperling (1987)[58] studied the effect of pH, ionic concentration, temperature, as well as the use of dried and hydrated corneal stroma on SP. Corneal stromas were dried to about 0.2 mm and constrained between two porous steel discs with no radial confinement in an immersion chamber where solute was added and the swelling force was measured using an electronic balance until the swelling force plateaued, this measurement was continuously repeated by incrementally increasing the corneal thickness by 0.1 mm. At a hydration of 3.4 mg H_20/mg dry wt.; a corresponding SP of 61.7±17.4 mmHg was reported.

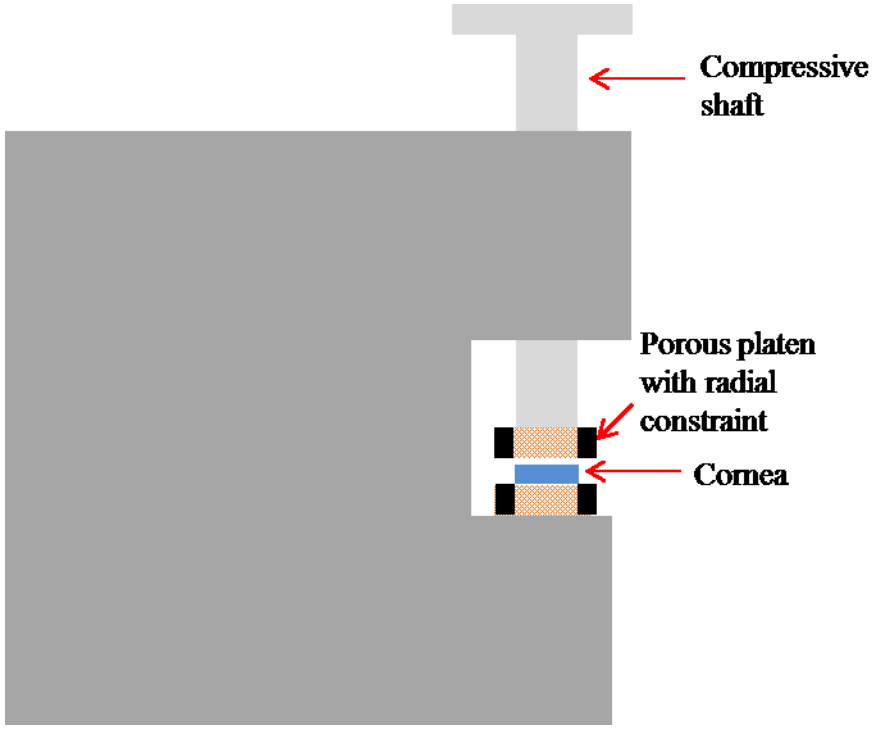

Figure 2.6: Schematic of experimental setup used in swelling pressure experiments. Cylindrical sample is confined with a porous ring and compressed.

The reported experimental observations from these tests provided vital information required for the production of corneal storage mediums for eye banks as SP provided a calibration pressure that was implemented osmotically using Dextran to prevent corneal swelling as well as validation for constitutive models for corneal swelling behavior[85, 89, 93, 94].

Studies by Eisenberg and Grodzinsky[95, 96] implemented confined compression and poroelastic modeling to characterize the confined compressive modulus, permeability, and stress relaxation behavior of bovine cornea hence combining corneal mechanics and transport behavior. In confined compression the outer edges of the cylindrical cornea is confined to prohibit radial displacements hence the loading conditions are purely compressive, the cornea is compressed by implementing a desired incremental compressive strain after which the transient behavior is observed over time; a confined compressive modulus of 34-58 KPa was reported. Kim et al.

studied the static compressive behavior of the cornea at strain rates in the range of accidental impacts using unconfined compression in a controlled humidity environment[97]. Strain rates ranging from 0.063/s to 50/s were applied to the cornea where rate dependent nonlinear stress-strain behavior was observed as the slope of the stress strain curve stiffened with increasing strain rate. At strain rate of 1/s, an initial tangential modulus of 0.243 MPa is reported.

2.3.2 Tensile, Indentation and Shear Tests

Uniaxial strip extentiometry tests are conducted on rectangular strips of cornea. Uniaxial strip extentiometry is either conducted in air or a submerged environment with corneal storage medium. Static instantaneous testing is commonly conducted using a constant displacement rate where stress strain behavior is characterized as a function of corneal anisotropy[10, 64, 65], displacement rate[65, 98], and species[30, 99]. Time dependent stress-strain studies are also conducted where the corneas transient response under constant strain or constant stress is characterized[10, 100-102]. The outcomes from these tests have reported to corneal stress strain behavior as nonlinear, viscoelastic, and hyperelastic. Furthermore at experimental stresses within physiological stress range, corneal behavior is reported as linear viscoelastic[100]. At higher levels of experimental stresses, corneal Young's modulus has been reported to be in the range of 40-57 MPa[13, 65, 103]. Biaxial inflation tests present a more physiological characterization technique to analyze the nonlinear viscoelastic and anisotropic behavior of the cornea. This technique is performed on excised corneas with a scleral rim[40, 86, 104-106] or on an intact corneo-scleral [107-110] where controlled external fluid is used to pressurize the corneas posterior and digital imagining is used to attain deformation of the corneal perimeter (see fig. 2.7).

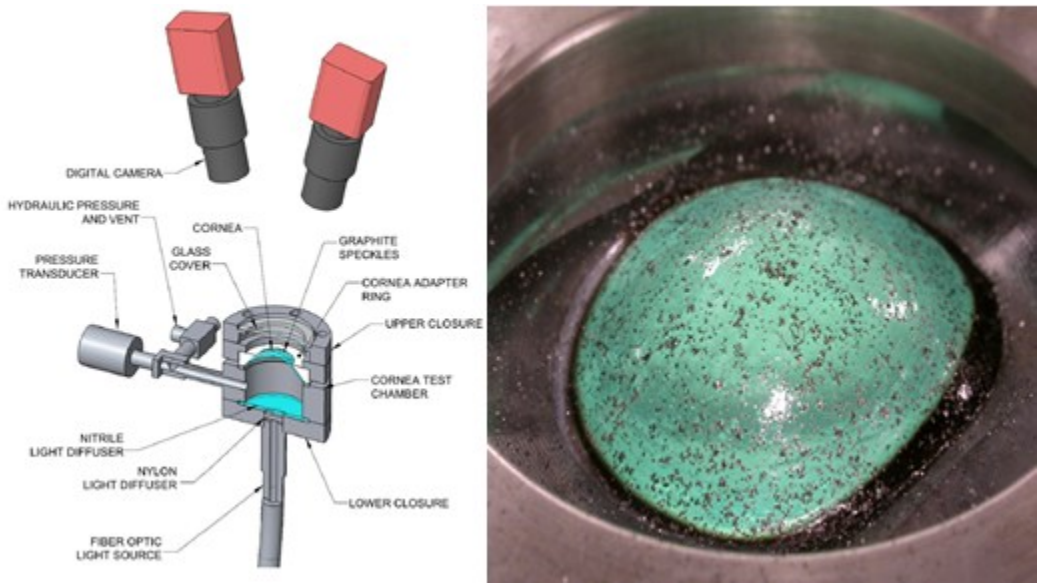

Figure 2.7: (Left) Schematic of experimental setup used in biaxial tensile tests. Posterior fluid pressure is applied to inflate the cornea and deformation is attained optically (Right) Picture of inflated cornea with grapheme particles for deformation analysis (with permission from [106]).

In biaxial inflation, the reported corneal Young's modulus ranges from 0.18-0.8 MPa at stresses within the physiological range and 3-22 MPa at stresses in the range of 6-77 KPa [86, 103-105, 107, 109].

Indentation techniques are also used to characterize corneal mechanics where an indenter is used to attain force displacement behavior for static and transient deformation behavior of the cornea. Experimental parameters such as the size of the indentation tip, indentation depth and loading rate have resulted in a wide range of reported Young's Modulus; the reported values range from 1.14 to 2.63 MPa [111] for the whole cornea, 2 to 15 KPa for the anterior basement membrane, 84 to 123 KPa for Bowman's layer, 20 to 80 KPa for the Descemet's membrane and 0.439 to 39 KPa for anterior, mid, and posterior stroma, [39, 112, 113].

Shear testing is a seldom method used to characterize corneal mechanics; however this method provides additional information on anisotropic corneal mechanics by characterizing shear modulus which cannot be attained from compressive, tensile or indentation testing techniques.

Soergel et al. (1995)[114] studied the shear mechanics of human corneas using oscillatory strain where the absolute value of shear compliance was observed to increase with parameters such as increasing frequency (-4 to 2 Hz), decreasing corneal thickness (1 to 0.2 mm), interval from post mortem to experimentation. Nickerson (2006)[115] reported storage modulus in the range of 0.6 KPa for porcine corneas using oscillatory stress (1 to 10 Pa) controlled rheometer at a frequency of 1 rad/s. Petsche et al . (2012)[1] reported shear modulus for anterior, mid, posterior and whole human corneas using oscillatory strain (1%) control at a frequency of 0.03 Hz where shear modulus was reported to increase with increasing compressive strain. Their reported values of storage modulus at initial cornea thickness are 7.7±6.34 Kpa, 1.99±0.45KPa, 1.31±1.01 KPa and 9.48±2.92 KPa for anterior, mid, posterior and whole corneas respectively.

2.4 Computational models for compressive corneal mechanics

Microstructural arrangement indicates the cornea is a porous media with liquid, solid, and ionic phases. A variety of numerical models have been developed or applied to characterize the behavior of the cornea.

2.4.1 Swelling models

Initial theoretical models applied to characterize the experimentally observed SP at varying hydrations/thickness and concentration was reported by Hart and Farrell (1971), as well as Elliot (1980)[116]. The model developed by Hart and Farrell described the mechanical SP as a function of GAG polymeric chain stretching in the stroma, excluded volume from the free energy of mixing based on the possibility of GAG chains colliding or GAG chain colliding with molecules from solution, polymeric solvent interaction and electrostatic interaction from the ionized GAGs[89].

Although this model considered the molecular interactions in the corneal stroma it was unable to predict the effects of ionic concentration, solvent type and temperature on the SP behavior as observed experimentally. Hodson's[12] theory of swelling was based on the notion that corneal SP observed mechanically is a function; (a) of the osmotic pressure difference between the interstromal fluid and the external immersion fluid $\Delta\pi$ (b) the outward tissue pressure P_t. Thus the SP observed mechanically is a combination of osmotic pressure and outward tissue pressure

$$SP = \Delta\pi + P_t \tag{2.1}$$

Observations from imbibition pressure experiments where a cannula is inserted into the cornea to measure its fluid pressure consequently rendering P_t absent; the measured SP using this method correlated with SP attained mechanically when the cornea is near physiological thickness. In this range of thickness P_t was deemed as negligible hence swelling pressure is generated solely from the osmotic pressure difference between the interstromal fluid and external immersion fluid; this is often referred to as the Donnan theory of corneal swelling. Donnan theory is expressed as a function of immersion fluid concentration and the concentration of the fixed charge in the stroma C_f; when the stroma is placed in NaCl immersion fluid. Osmotic pressure is expressed as a function of gas constant R, temperature T, and concentration of the sodium ions Na_0.

$$\Delta\pi = RT\left(\sqrt{C_f^2 + 4Na_o^2} + 2Na_o\right) \tag{2.2}$$

This theory is able to predict the behavior of corneal SP at thickness within physiological range however at thicknesses below physiological thickness it is limited[58]. Furthermore, the effect of increasing bath concentration by 10 folds from physiological concentration of 0.15 M has not been shown to abolish stromal swelling[88]. Additional swelling models based on Poisson-Boltzmann equation was used to attain the stromal charges with the implementation of volume exclusion for the collagen fibrils with the decrease in corneal thickness[117]. In this model SP is

expressed as a function of stromal volume V_s, and Helmholtz free energy Γ at fixed temperature and pressure; where Γ is divided into electrostatic and chemo-mechanical parts.

$$SP = -\frac{\partial \Gamma}{\partial V_s}\Big|_{T,P} \tag{2.3}$$

This model was able to predict corneal SP at all thickness ranges; characterization of the stromal charges as function of charges from interfibrillar volume and collagen fibril coating was also shown to improve the models prediction.

2.4.2 **Biphasic model**

Linear biphasic theory has been implemented to describe cartilages response in compression[118, 119]. In this theory, the time dependent responses of a tissue with solid (collagen, proteoglycan, and cells) and fluid (water) phases are dependent on the dispersion of interstitial fluid drag though the porous solid phase; this theory has been implemented to successfully describe transient cartilage mechanics under constant stress or strain[118-123]. Similar to the cornea, the cartilage is also composed of water, collagen and negatively charged proteoglycans however their structure and relative content of these constituents vary. Using linear biphasic theory with the addition of third phase, Eisenberg and Grodzinsky[95, 96] modeled the cornea as porous material composed of solid, interstitial fluid and a chemically charged phase that generates chemical stresses (σ_{ch}). Solid phase was assumed as linear elastic, and the interstitial fluid was assumed as intrinsically incompressible, and inviscid. Using Darcy's law with the inclusion of (a) osmotic and hydrostatic pressure, (b) equilibrium conditions of no fluid flow inside or across the cornea, (c) the relation between fluid velocity, permeability and fluid pressure P_{fl}. The total stress on the cornea during confined compression with the application of uniaxial strain (ϵ) is given in equation 2.4; where confined compressive modulus $H_A(c)$ and chemical stress material parameters display ionic

concentration dependence. When constant stress or strain is applied over time, P_{fl} dissipates thus resulting in an equilibrium response solely dependent on $H_A(c)$ and σ_{ch}.

$$\sigma_{M\_tot} = P_{fl} + \sigma_{ch} + H_A(c)\epsilon \quad (2.4)$$

Although this model takes into consideration the multiphasic nature of the cornea, it does not account for anisotropy based on the application to confined compression. Similar mixture models based on Armstrong et al. (1984)[119] has been applied to characterize engineered corneal stromal equivalent[18].

CHAPTER III

EXPERIMENTAL INVESTIGATION OF THE COMPRESSIVE MECHANICAL PROPERTIES OF PORCINE CORNEAL STROMA

Mechanical properties of the cornea determine its deformation behavior when stress is applied, knowledge of corneal mechanics is essential for the development of constitutive models that can be possibly applied in surgical reshaping and clinical device applications[124-126]. In post mortem conditions when whole or excised corneas are used for mechanical characterization, the cornea swells which leads to non-physiological state of hydration/thickness[6, 48, 116]. Thus far, the common *ex vivo* corneal characterization techniques such as uniaxial strip extentiometry, and biaxial inflation do not provide the ability to experimentally vary corneal thickness[98, 100, 101, 104, 106]. The state of corneal hydration/thickness is reported to alter mechanical properties of the cornea[107, 127, 128]. Furthermore, loading rates, temperature, experimental immersion fluid, and ionic concentration of immersion fluid have also been seen to affect the response of cornea under stress. Majority of corneal mechanics studies have been focused on its tensile properties as the cornea is always in biaxial tension from internal loading due to IOP. However, external loading from atmospheric pressure, closed eyelids, and applanation of external objects results in application of compressive loads. Due to the anisotropic nature of the cornea, these compressive loads are applied outside the plane of collagen alignment, thus the response of cornea to compressive loads differ from its tensile response. Moreover, knowledge of the corneal compressive properties could be essential to assessing the effect of disease to the extrafibrillar matrix.

A compressive testing technique known as unconfined compression has been applied to characterize the mechanics of other soft tissues such as the sclera, cartilage, brain[119, 129, 130]. Unconfined compression is generally conducted on a cylindrical sample compressed in uniaxial compression between two smooth impermeable platens in a submerged environment where lateral (radial) expansion is unconstrained; this results in application of compressive loads in the axial (compressive) direction. This technique has been used to characterize compressive modulus and rate dependent properties; furthermore analytical and numerical models have been developed based on unconfined compression to attain the materials permeability and tensile modulus based on anisotropy and radial expansion[121-123, 131, 132]. An additional benefit of unconfined compression in characterizing corneal mechanics is the ability to fully control the hydration/thickness of the cornea, thus corneal mechanics can be characterized at varying thicknesses.

In this study, unconfined compression will be employed to study the compressive response of the cornea. Effects of experimental conditions such as rate dependent loading, use of freeze-thaw samples, testing temperatures as well as the effect of sample diameters will be examined. It is noted that the effect of experimental conditions were not fully characterized due to the lack of time. Therefore, the pertinent data should only be regarded as preliminary results; future studies are required for proper understanding of their possible influence on corneal mechanics.

3.1 Sample preparation

Porcine eye globes were attained from a local abattoir within 1 to 4 hours and transported in plastic bags positioned in a cooled chest. The corneal surface was optically examined for scratches and swelling, corneas free of scratches and swelling were excised[25]. Prior to excision the thickness of each cornea was measured with a pachymeter (DGH Pachette 3, Pennsylvania). An incision below the corneoscleral junction was created with a scalpel, and then micro

dissecting scissors (Biomedical Research Instruments, Inc. MD) were used to excise the cornea with a scleral rim. The corneal endothelium and epithelium were rubbed off using a dull scalpel and Kim wipes[134 ,133]. Circular trephines of diameters 10 mm, 8 mm, 6 mm and 4 mm were used to punch out stroma from the central region. Trephined stromas were weighed using an analytical scale of 0.1 mg accuracy (Torbal Analytical Balance, New Jersey) followed by thickness measurements using a pachymeter (DGH Pachette 3, Pennsylvania). Freshly trephined stromas were immediately used for unconfined compression tests, while stromas not in current use were wrapped in cling film to preserve its hydration and frozen at -20°c[135].

3.2 Compressive Mechanical testing

A DHR-2 Rheometer (TA Instruments, Delaware) equipped with a true position sensor and a 50 N load cell with sensitivity of 5 mN was used to conduct unconfined compression. Additional rheological accessories such as an environmental controlled submersion kit attached to a peltier with a parallel surface, and a top stainless steel parallel plate geometry 20 mm in diameter with a smooth impermeable were used to conduct all experiments in this study. The rheometer was calibrated to attain a zero gap position in the immersion fluid at the desired experimental temperature using TRIOS software (TA Instruments, Delaware), furthermore this software was also used to collect experimental data at a frequency of 1Hz.

Figure 3.1: Experimental setup showing the DHR-2 rheometer connected to TRIOS software during unconfined compression.

3.2.1 Strain rate dependent corneal behavior

Unconfined compression was conducted by immersing corneal stromas (10 mm diameter) in 0.9% NaCl for 60 minutes in order to reduce the rate of corneal swelling prior to mechanical loading. After the 60 minute equilibration period, corneal stromas were placed directly underneath the middle of compressive top parallel plate geometry in a submersion chamber of the rheometer filled with 0.9% NaCl set at a temperature of 37±0.1° C. In order to attain a reference point for all experiments, a tare stress of 1.5 KPa was applied for 30 minutes; thickness of the cornea after equilibration at 1.5 KPa was used as the starting thickness for all strain calculations. Stress was calculated as the measured force divided by the un-deformed sample area. Once the sample thickness at tare stress was attained, infinitesimal compressive strains of 4% was applied using a displacement rate of 0.15 μm/s, after which stain was kept constant for 30 minutes to observe the corneal time dependent behavior until the transient stress equilibrated. This procedure was repeated until 20% stain was attained in five cycles. Additional strain were applied using larger strain increments of 10% strain to attain 30%, 40% and 50% compressive strains tailed by constant strain period for 30 minutes.

To determine the effect of strain rate on corneal mechanics, varying displacement rates were used to conduct unconfined compression tests on 10 mm samples. IOP has been reported to vary with body position[136], Linder et al (1988)[137] reported a 3 fold increase of IOP *in vivo* when the head is inverted against gravity in comparison to an upright position, supine position was also reported to increase IOP. In previous work by Mattson et al (2010)[110], enucleated intact eye globes were pressurized to physiological IOP of 22 mmHg, after which the corneal perimeter was monitored optically for 15 minute intervals. The average corneal perimeter displacement rates are reported as 0.73 μm/s and 0.2 μm/s after 15 and 30 minutes respectively, this provided *in vivo* corneal displacement rates in the event of IOP change. Based on this report displacements of 1 μm/s (n = 5), and 0.5 μm/s (n = 6) were used to conduct unconfined compression experiments on 10 mm samples.

The total time for a single experiment was within 5 to 6 hours. Due to the length of experimental time and the steady availability of corneas, it was of essence to characterize the effect of corneal storage by freezing on corneal mechanical behavior. Freshly trephined (n = 5) and frozen (n = 8) corneal stromas, all of diameter 10 mm were subjected to the loading conditions described above using a displacement rate of 0.15 μm/s, to determine the possible effects on freeze-thaw samples. Frozen samples were kept in the freezer for up to 1-2 weeks. Frozen samples were thawed at room temperature for 30 minutes, reweighted and thickness measured. This was followed by immersion 0.9% NaCl similar to fresh stromas.

Cylindrical corneal stromas of diameters ranging from 13.5 mm to 5 mm were used to characterize corneal behavior in previous works, the effect of sample diameter was considered minor as samples of varying diameters produced similar stresses. Nevertheless, these studies only reported the effect of varying sample diameter on transient mechanics, thus it was of essence to investigate the effect of sample diameter on instantaneous mechanics.

To determine the effect of sample diameter on the observed mechanical response attained from corneal stromas, smaller samples of diameter 8 mm (n = 4) were attained from the corneal central region. The immersion fluid, soak time, tare stress, applied displacement rate, and strain increment used to apply incremental strains from 4% to 50% compression as described previously for experiments conducted on 10 mm diameter samples using a displacement rate of 0.15 μm/s.

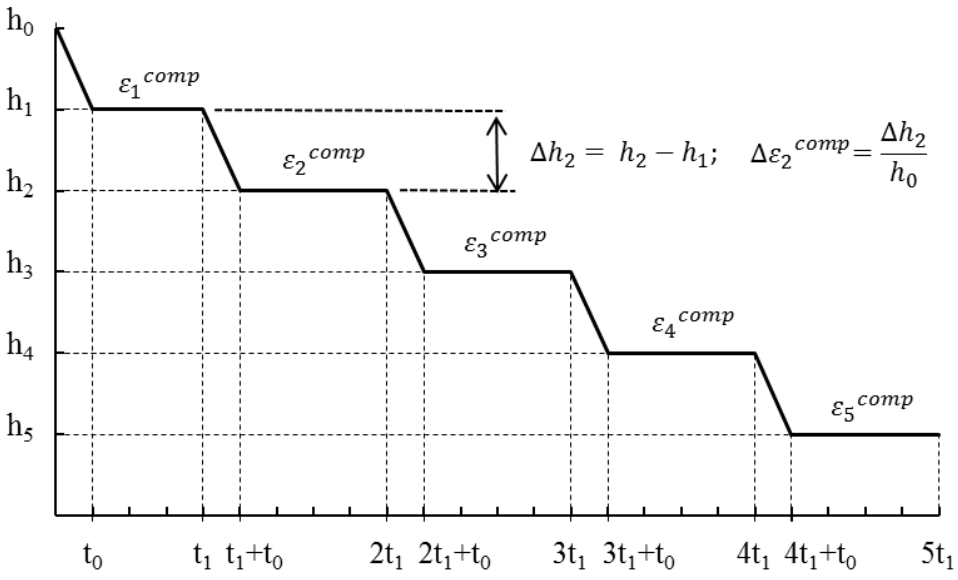

Figure 3.2.1: The transient displacement of corneal stroma during stepwise unconfined compression-stress relaxation experiment.

3.2.2 Effect of corneal thickness on corneal behavior

Stiffness, extensibility, and viscoelasticity of the cornea have been reported to be influenced by the level of hydration/thickness of the cornea[107, 127]. Furthermore, diseases such as Funch's dystrophy and Bullous Keratopathy were reported to increase corneal thickness, where up to 10% increase in corneal thickness on average were observed. Thus it was of essence to characterize the

effect of normal and swollen corneal thickness on corneal mechanics. After the equilibration of 10 mm trephined stromas in 0.9% NaCl for 30 minutes, unconfined compression tests were conducted by applying tare stress for 30 minutes. Two categories of tare stresses were applied to attain varying sample thicknesses; a tare stress of 7.2±0.5 KPa was applied to attain stromas in the range of physiological thickness, while a tare stress of 1.9±0.18 KPa was applied to attain corneas above physiological thickness. Based on the thickness after tare stress 4% compressive strain was applied followed by constant strain for 30 to 45 minutes. The effect of viscoelasticity as examined by applying varying displacement rates of 0.15 μm/s (n = 5), 0.5 μm/s (n = 5) and 1 μm/s (n = 5) for each tare stress criteria resulting in a total of 15 tests at each thickness category.

3.2.3 Thermal effects on corneal mechanics

The possible effects of thermal variation on corneal mechanics was studied by conducting unconfined compression tests at temperatures of 25°C (n = 4) and 40°C (n = 4). In the case of high fever, the body temperature is reported to increase up to 40°C. Moreover previous compressive studies reported a variation in the equilibrium stress with change in temperature[90, 138]. Fatt (1971), reports a decrease in thickness of up to 100 μm when corneal stromas compressed between two porous filters tested at 25ºC were compared to 37°C at equilibrium compressive stresses ranging from 1.3 to 13.3 KPa. Hara and Maurice (1972) measured corneal equilibrium stress by applying suction to corneas placed between porous surfaces where stabilization in the change in volume was used to determine equilibrium; temperature regulated bath was employed to determine the effect of temperature on equilibrium stress where decrease in temperature was observed to result in an absolute increase in the value of equilibrium stress by 0.27 to 1.3 KPa for temperature increase of 10°C.

Unconfined compression was conducted on trephined stromas of 10 mm diameter employing similar immersion fluid, soak time, tare stress, applied displacement rate, and strain increment used to apply incremental strains from 4% to 50% compression as described in section 3.2.1 where 10 mm samples were tested at 37°C using a displacement rate of 0.15 μm/s; nevertheless modifications were made to the thermal settings of the environmental submersion chamber to attain experimental temperatures of 40±0.1°C or 25±0.1°C.

3.2.4 Statistical Analysis

One way or two way ANOVA with replication were employed to assess the effects of freezing, compressive strain, sample diameter, displacement rate, temperature, and corneal thickness where statistical significance of $p<0.05$ was applied to all statistical analysis.

3.3 Results and Discussion

In the constant ramp strain region, corneal stromas displayed a nonlinear transient stress increase until strain was kept constant after which the transient stress was observed to relax to an equilibrium value. Incremental increase in compressive strain amplified the value of peak stresses observed during ramp strains as well as the equilibrium stresses attained after relaxation (See fig. 3.3.1). The peak and equilibrium stress-strain behavior displayed nonlinearity; a peak tangential modulus was calculated based on the incremental increase in strain from 0 to 50% using the average peak stress at each strain increment. A similar method was employed to calculate the equilibrium compressive modulus using an average equilibrium stress at each strain increment.

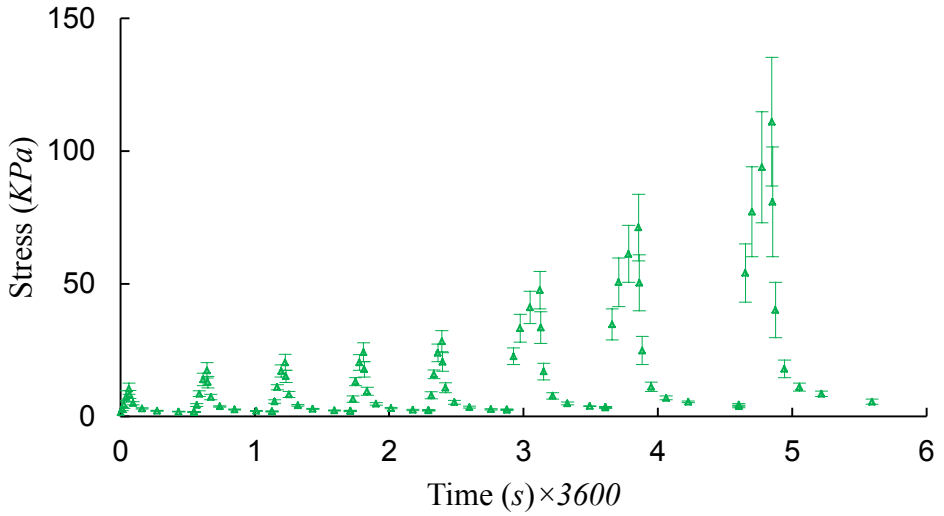

Figure 3.3.1: The average transient stress attained from 10 mm samples unconfined compression at displacement rate of 0.15 µm/s. Few points selected for clarity. Error bars indicate (±1 S.D.).

3.3.1 Effect of displacement rate

Instantaneous response of the cornea during loading with constant displacement rate displayed an increase at higher displacement rate as maximum stress attained were amplified by intensifying displacement rate from 0.15µm/s to 1µm/s across all compressive strains tested. This variation in peak stress was statically significant from 0.15µm/s to 0.5µm/s across all compressive strains where the attained peak stress was at least two times greater as seen in table 3:3.1. However; the increase in displacement rate from 0.5µm/s to 1 µm/s was not statistically significant for strains between 0-20%. Nevertheless a significant variation was observed from 30-50%. Unlike the instantaneous response, the time dependent response was not affect by displacement rate as it was observed that at each compressive strain increment, equilibrium stresses were similar.

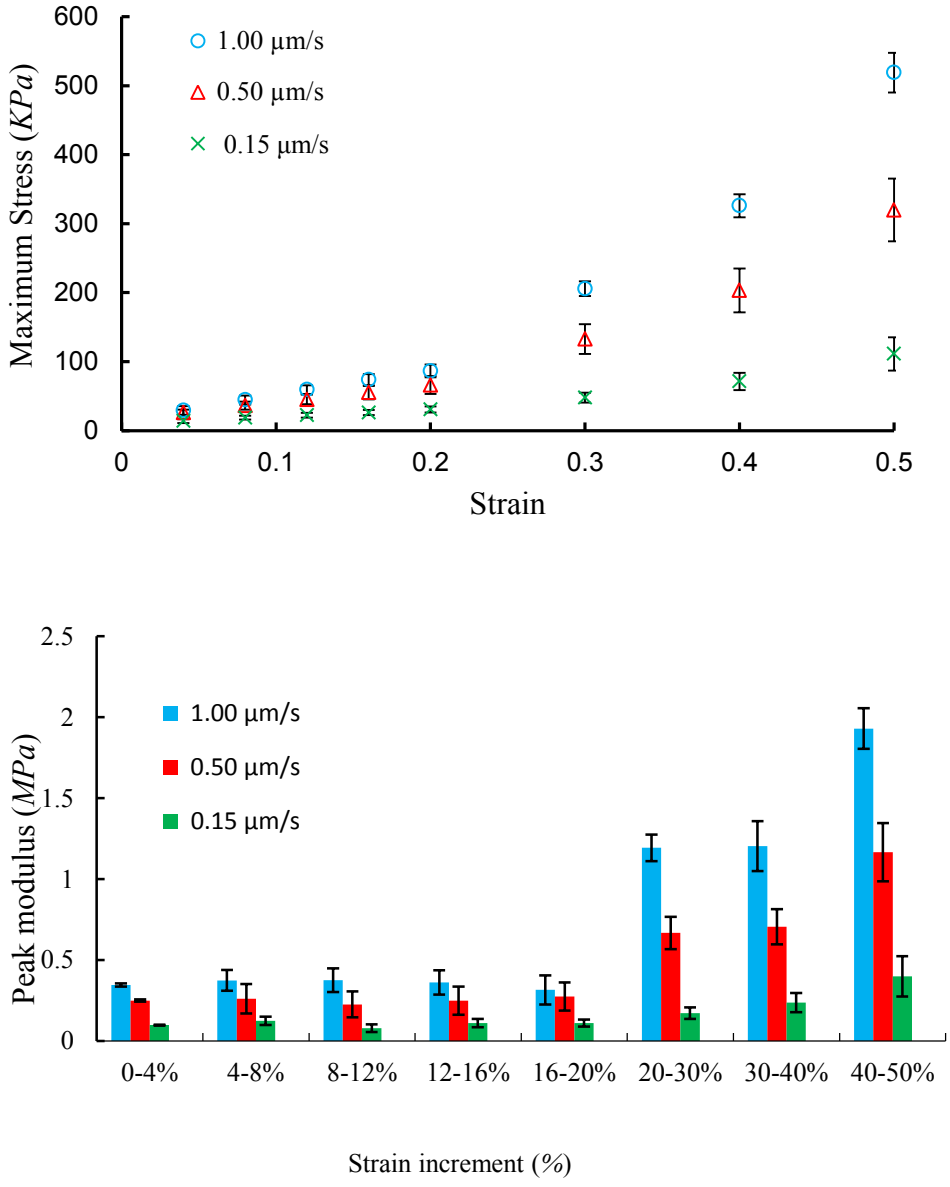

Figure 3.3.2: (Top) average peak stress strain relationship attained displaying an increase in peak stress with increasing displacement rate (Bottom) effect of displacement on the peak modulus behavior attained with varying displacement rate.

Displacement rate has been reported to affect instantaneous response of the cornea in compression; Kim et al. (2012) attained stress-strain relationships from bovine corneas using strain rates ranging from 0.063/s to 50/s where stiffening behavior was observed with increasing

strain rate, this behavior is as also observed in the current study, but the effect of displacement rate on the time dependent response were not studied until this work[97]. In the current study it is observed that the time dependent stress response of the cornea dissipates to constant value at the same strain increment independent of displacement rate. This indicates the cornea could possibly displays flow independent viscoelasticity during the ramp phase of unconfined compression due to intrinsic solid viscoelasticity and flow dependent viscoelasticity at constant strain as a result of mechanical consolidation from the flow of fluid through the cornea as observed in the response of cartilage and other soft tissues in unconfined compression[119, 123, 139]. Based on this observation, it would be beneficial to fit the transient stress to biphasic flow dependent models as well as the inclusion of fluid flow to analytical and numerical models used in corneal mechanics[140].

Table 3:3.1: The effect of displacement on the average peak compressive modulus.

	Disp. Rate (μm/s)	0-4%	4-8%	8-12%	12-16%	16-20%	20-30%	30-40%	40-50%
Peak	0.15	0.1±0.00	0.19±0.03	0.09±0.02	0.1±0.02	0.11±0.02	0.19±0.04	0.24±0.06	0.4±0.12
Modulus (MPa)	0.5	0.25±0.01	0.26±0.09	0.22±0.08	0.25±0.09	0.27±0.09	0.67±0.1	0.7±0.11	1.17±0.18
	1	0.34±0.01	0.37±0.06	0.38±0.07	0.36±0.08	0.32±0.09	1.19±0.08	1.2±0.15	1.93±0.13

A comparison of the stress-strain relationship using freeze-thaw samples and fresh samples displayed no significant difference in the equilibrium stress, maximum stress, equilibrium modulus and peak modulus attained from fresh and frozen samples (fig. 3.3.2); table 3.3.2 summarizes the p values of this analysis. In fresh samples it is observed that the change in compressive modulus with increasing compressive strain is not statically significant ($p=0.08$), however there is significant increase at 50% strain ($p<0.05$). A similar trend is observed for the peak modulus as it does not vary significantly from 0-40% ($p=0.10$) after which there is a

significant increase at 50% strain ($p<0.05$). For freeze thaw samples, a comparison on the effect of compressive strain on compressive modulus indicates there is no statistical difference ($p=0.43$) for compressive strains less than 30%, however the compressive modulus attained at 40% displays a statically significant increase ($p<0.05$) with respect to values attained from 0-30% compressive strain. Further increase in strain to 50% displays a statically significant change ($p<0.05$) in compressive modulus. A similar pattern is also observed in the variation peak modulus behavior from 0-50%.

Previous compressive studies on the cornea where the equilibrium compressive stress behavior was studied, reported no variation in the equilibrium stress attained from fresh and freeze-thaw samples[46, 47, 58], this is conjunction with the current observation. In addition, the current work shows freezing and thawing did not affect the transient stress behavior during instantaneous compression and stress relaxation as the peak stresses or the shape of the transient stress did not vary after freeze thaw in comparison to fresh samples.

Table 3.3.2: A comparison of the average peak stress and peak modulus attained using fresh (F) and frozen-thaw (F-T) corneal stromas.

	State	0-4%	4-8%	8-12%	12-16%	16-20%	20-30%	30-40%	40-50%	p value
Inst. Stress (KPa)	F	14.3±2.6	18.3±2.5	21.3±2.7	25.2±3.4	29.4±3.9	49±7.4	73±13.4	114.2±26.2	0.06
	F-T	14.3±2.6	18.3±2.5	21.3±2.7	25.2±3.4	29.4±3.9	49±7.4	73±13.4	114.2±26.2	
Peak comp. modulus (MPa)	F	-	0.17±0.13	0.13±0.04	0.12±0.06	0.1±0.05	0.22±0.05	0.26±0.06	0.42±0.13	0.99
	F-T	-	0.12±0.02	0.08±0.01	0.1±0.03	0.11±0.03	0.2±0.04	0.24±0.07	0.39±0.14	

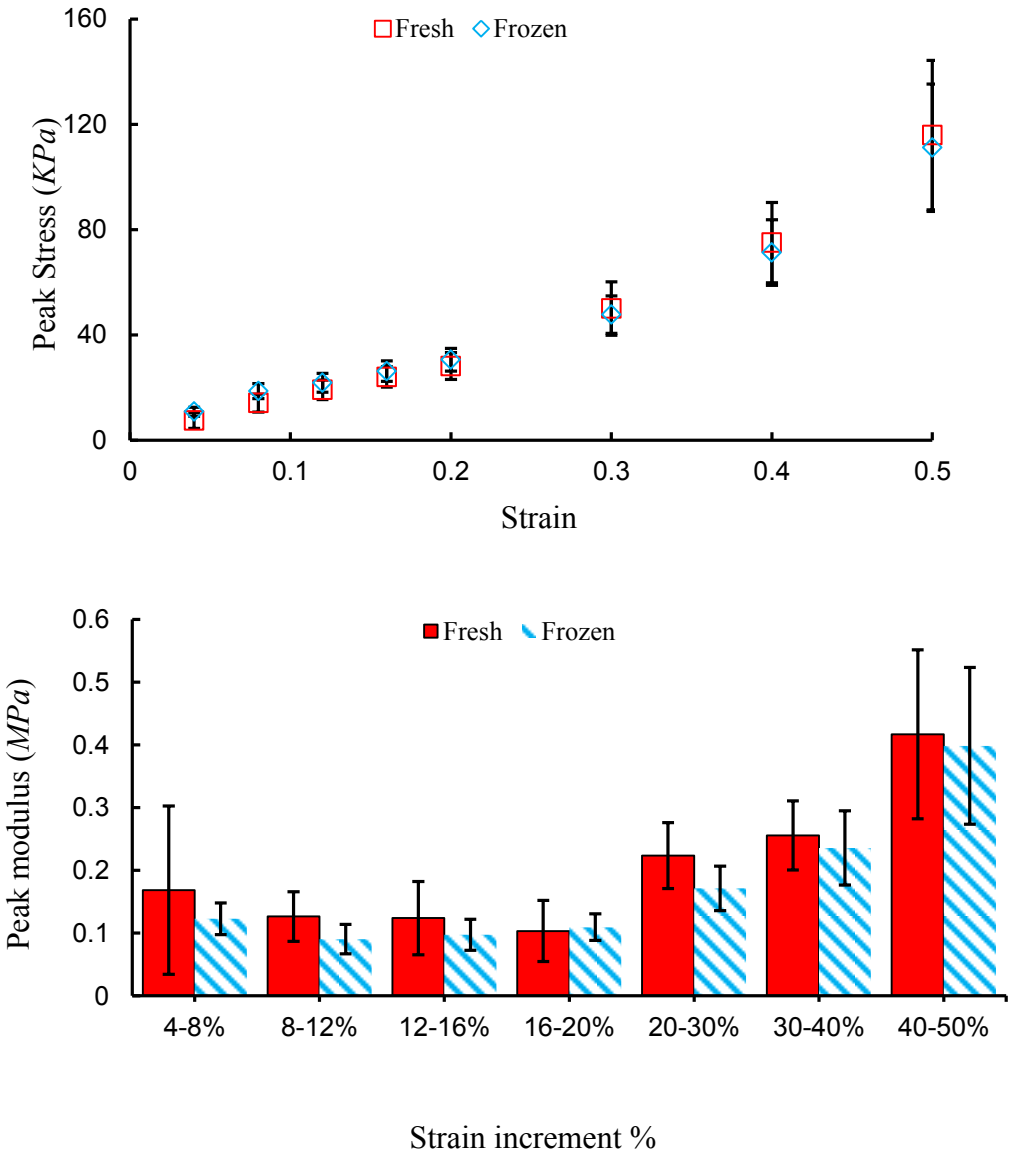

Figure 3.3.3: The average (Top) peak stress (Bottom) peak compressive modulus attained at varying compressive strain increments for fresh and frozen samples.

A comparison of equilibrium stress attained from 8 mm and 10 mm samples did not display any significant variations across all strain increments ($p=0.21$). Peak stresses achieved from 10 mm and 8 mm samples did not vary significantly ($p=0.255$); there was also no variation in the peak modulus calculated between samples of 10 mm and 8 mm diameters ($p=0.49$).

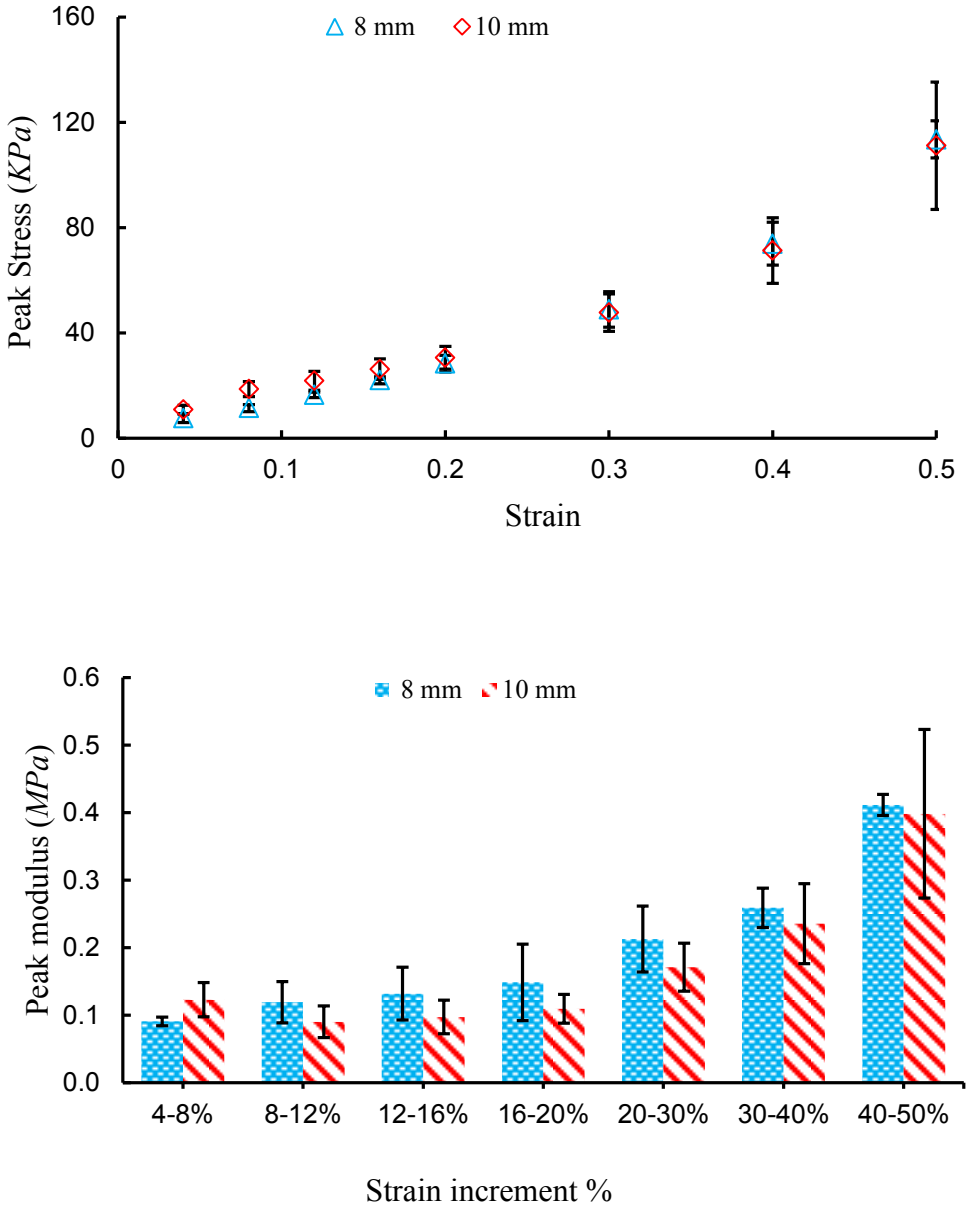

Figure 3.3.4: The average peak modulus relationship attained using varying corneal stroma button diameters of 10 mm and 8 mm.

Effect of sample diameter on equilibrium stress response of the cornea has previously reported as trivial by previous studies[46, 58], where Hedbys et al (1963) did reported no appreciable difference with sample diameter varying as samples of 6.5 mm, 9.0 mm and 13.5 mm diameters were employed in their work. In addition, Olsen and Spearling (1987) also reported identical values of equilibrium stress were attained from 7 mm and 5 mm samples. This behavior is also observed in

the current study. The peak stress response was not observed to be affected by sample diameter as the peak stress attained from samples of diameters 10 mm and 8 mm were similar. Although samples of diameter less than 8 mm were not used in this study, we anticipate a reduction in peak stress with the reduction of sample diameter.

3.3.2 Effect of Corneal thickness

At high and low thicknesses, the corneal stroma displayed viscoelastic behavior during the ramp and stress relaxation phase of unconfined compression. In the ramp phase, peak stress increased with increasing displacement rate while stress dissipated during constant strain. Instantaneous stress-strain response was affected by displacement rate as stiffness increase was attained for higher displacement rates. In the linear region, swollen corneas displayed values of Young's modulus ranging from 0.4 to 1.49 MPa, while the corresponding Young's modulus range from 1.42 to 4.89 MPa for corneas at physiological thickness; higher range of Young's modulus corresponds to values attained from experiments conducted at displacement rate of 1 μm/s. The maximum stress attained at 4% compression from swollen corneal stromas during instantaneous compression using displacement rates of 0.15 μm/s, 0.5 μm/s and 1 μm/s are 19.8±3.46 KPa, 43.1±6.8 KPA, and 57.4±6.2 KPa respectively. These values are significantly less than the corresponding maximum stresses of 74.0±17.4 KPa, 113.2±19.5 KPa, and 140.4±37.6 KPa using a tare stresses of 7.2±0.5 KPa where the cornea is in the range of physiological thickness.

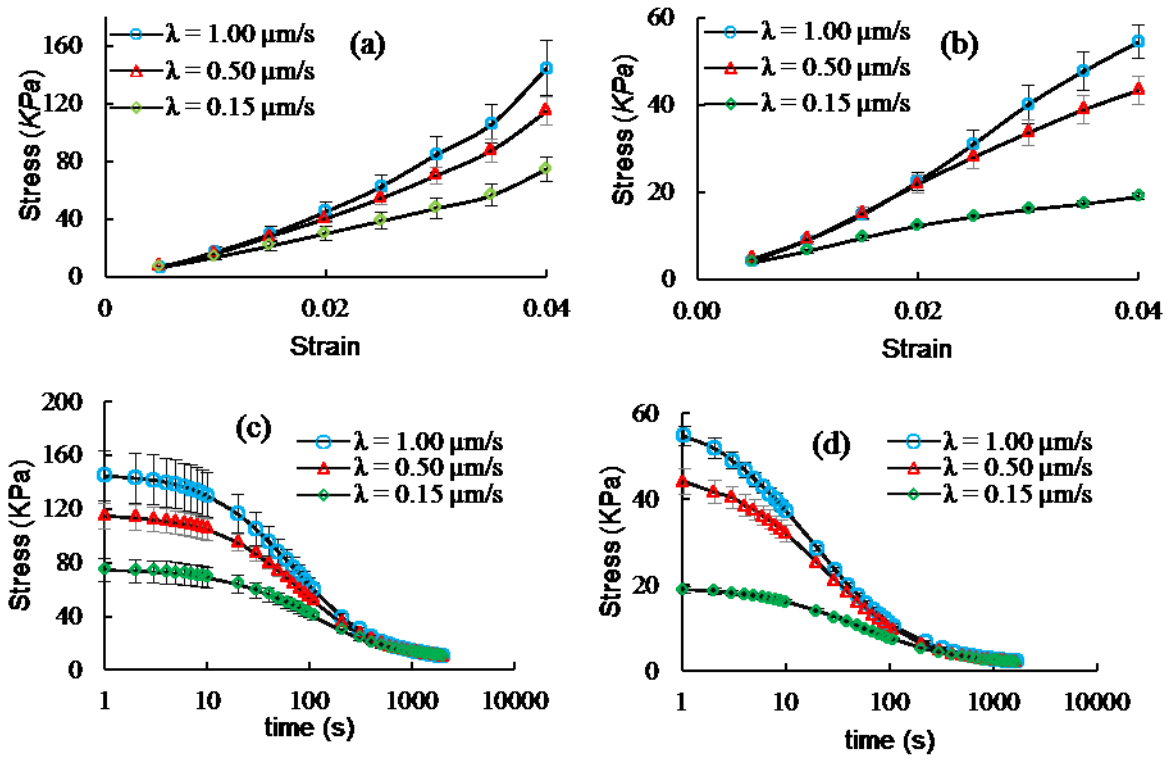

Figure 3.3.5: The effect of displacement rate on the average instantaneous stress-strain relationship for corneas of (a) normal thickness (b) swollen thickness. Transient dissipation of stress attained from (c) normal thickness (d) swollen thickness.

At a tare stress of 1.9±0.18 KPa where the corneal stroma is swollen, an average equilibrium compressive modulus of the corneal stroma is irrespective of strain is 22.3±9.6 KPa, this is significantly less than the average equilibrium compressive modulus of 46.1±22.6 KPa attained when cornea thickness is close to physiological levels.

The variation of corneal thickness using two different tare stresses is shown to affect the level of axial (out of plane) displacement as at a constant instantaneous stress, the cornea is observed to display higher levels of strain for corneas tested at 1.9±0.18 KPa tare stress in comparison to 7.2±0.5 KPa. The use of 7.2±0.5 KPa to attain corneas at physiological thickness is justified by an average thickness of 687±24 μm after tare stress equilibration, which is within the range of

physiological thickness reported as 666±68 μm by Faber et al. (2008)[21]. The instantaneous stress-strain relationship for swollen and normal corneas display non-linear viscoelastic behavior as also reported by Kim et al. (2012)[97] where the slope of the stress-strain curve is given as 0.243 MPa at strain rate of 1/s. In the current study the displacement rate of 1μm/s correspond to strain rates of 8.81×10^{-4}/s and 1.43×10^{-4}/s for swollen and normal thickness corneas; the initial slope of the average stress strain curves are 1.2 MPa and 2.3 MPa respectively. These values are up to 10 times the magnitude reported by Kim et al (2012), however experimental differences in the current study corneas were immersed during experimentation while Kim et al. (2012) used a humidity chamber to maintain corneal dehydration during testing thus the possible effect of evaporation may have affected the instantaneous response of the cornea.

Additional differences could also be due to the use of species as Kim et al. (2012) used bovine corneas where preferential orientation of collagen fibrils is in IS direction in comparison to the circumferential preferential orientation displayed porcine corneas[73]; the preferential circumferential arrangement plays a role in restricting the radial expansion thus the preferential circumferential orientation may result in higher stress response during compression.

The equilibrium compressive modulus attained for swollen and normal thickness corneas are 22.3±9.6 KPa and 46.1±22.6 KPa respectively. The average compressive modulus of corneas at physiological thickness are reported to be within 39-40 KPa by previous studies which is within the magnitude reported in the current study[1, 58, 95].

3.3.3 Effect of test temperature

A comparison of stress strain relationship attained from experiments conducted at 40°C, 37°C and 25°C, shows that the average equilibrium stress attained across all strain increments does not

vary significantly (p=0.50); a similar trend is also observed from the resultant equilibrium compressive modulus (p=0.56).

Peak stress does not display statistical difference (p=0.92) from 4% to 50% strain for experiments conducted at 40°C, 37°C and 25°C; the corresponding peak modulus does not vary significantly (p=0.94) within this temperature range. Average peak modulus attained at 4% to 50% strain at 25°C, 37°C, and 40°C range from 0.09-0.6 MPa, 0.07-0.4 MPa, and 0.08-0.4 MPa respectively, where lower regions of peak modulus are attained at lower compressive strains.

At test temperatures of 25°C to 40°C minute variation in peak and equilibrium stress were observed; similar trend was observed for the peak and equilibrium modulus. The effect of temperature on equilibrium stress was previously reported by Hedbys et al. (1963)[46] where experiments conducted at room temperature and 4-6°C displayed similar values. Moreover Olsen and Sperling (1987)[58] reported no spastically significant difference between tests conducted at room temperature and 37°C. The observations of temperature independence from 25°C to 40°C on equilibrium stress are in conjunction with previous reports.

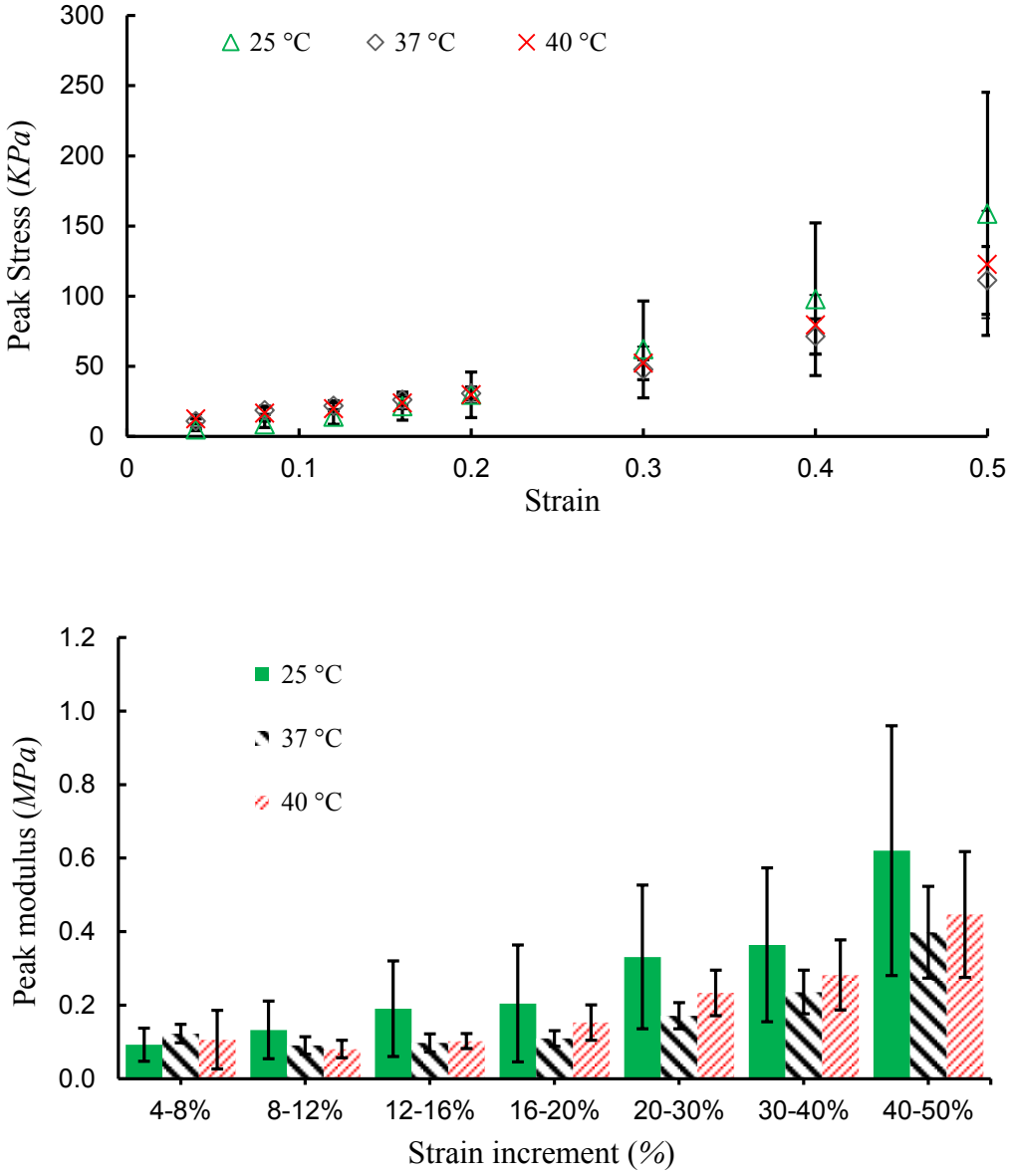

Figure 3.3.6: The effect of experimental testing temperature on (Top) peak stress and (Bottom) peak modulus across all strain increments.

Limitations in the current experimental study include flattening the native corneal curvature to a planar state thus resulting in pre-stressed state before experimentation. A planar sample is required to maintain proper contact between the cornea surface and the compressive geometries of the rheometer thus this was unavoidable based on the current experimental technique. Due to

the length of experiment conducted from 4-50% strains, some evaporation occurred during the experiment. This was countered by addition of water at prescribed time intervals to the environmental controlled immersion chamber based on the rate of evaporation measured prior to experimentation for a given temperature and molarity of NaCl immersion fluid.

CHAPTER IV

BIPHASIC ANALYTIC AND NUMERICAL MODELLING OF THE CORNEAL STROMA

4.1 Goal

Mechanical and transport behavior of the cornea can be predicted with a combination of data attained experimentally and realistic theoretical models. There are a variety of theoretical models that are used to predict the mechanical behavior of the cornea; however these models do not consider the corneas multiphasic nature or anisotropy. The cornea is a semi-permeable load bearing connective tissue that consists mostly of highly organized fibrillar network, negatively charged proteoglycans and water. When mechanical or chemical loads are applied on the cornea, stresses are generated in the solid phase, hydrostatic pore pressure in the fluid phase and osmotic pressure is generated due to negatively charged proteoglycans. Most of the current models that have been applied to describe corneal mechanical behavior account for structural anisotropy of the solid collagen phase; where corneal matrix is modeled as an incompressible solid using a combination of hyperelastic strain energies. From a structural standpoint, these models fail to account for the semi-permeable nature of the cornea as well as the interaction of its fluid and solid phase. Except for models implemented by Boyce et al. (2007)[100], the experimentally observed viscoelasticity is also omitted from these hyperelastic models. Furthermore, in compression, corneal mechanical behavior displays fluid flow viscoelasticity, thus it is of essence to implement a multiphasic approach to realistically model corneal mechanics when loads in the

out of plane direction are applied as seen in applanation of external objects such as clinical, surgical devices[141, 142]. Grodinsky and Eisenberg[95, 96], implemented a multiphasic approach to account for the stresses in the solid and fluid phase as well as the chemical stresses generated by chemical stresses based on the linear biphasic theory developed by Kuei, Lai, and Mow (1980) for the cartilage. This model did not account for corneal anisotropy as the solid phase was modeled using isotropic linear elasticity, besides Grodinsky and Eisenberg (1987) employed confined compression in their experiments thus loading was only applied in 1-D. Using a similar approach, a biphasic model that accounts for anisotropy will be implemented to experimental data attained from unconfined compression where the cornea is under compressive conditions. The application of biphasic models to unconfined compression was initially implemented by Armstrong, Lai, and Mow (1984)[119] for the cartilage where isotropic linear elasticity was used to model the solid phase however this model was unable to reproduce the high peak stresses observed in experimentation. This model was later modified by Cohen et al (1998)[121], by implementing transversely isotropy to the solid phase where the transversely isotropic biphasic model was able to fit the experimentally observed peak stresses for growth plate and chondroepiphysis.

4.2 Experimental data source

Experimental data for unconfined compression of porcine corneas were attained from chapter 3.

In this chapter, we hypothesize that the porcine cornea is transversely isotropic material, the plane of isotropy is the in-plane direction where the collagen fibrils are circumferentially oriented and anisotropy occurs through the thickness. A transversely isotropic biphasic model is implemented to describe the transient stress behavior of the cornea during unconfined compression, when constant compressive strain rate is applied followed by constant strain rate. The transversely

isotropic model will be described and a closed form solution provided. A finite element model of the cornea based on transversely isotopic biphasic properties will be created and compared to the closed form solution.

4.3 Transversely Isotropic Biphasic Model

In biphasic theory, hydrated soft tissues are designated as a binary mixture of a distinct fluid and solid phase, these phases are assumed to be homogenous, non-miscible, and incompressible[119]. The total stress ($\boldsymbol{\sigma}^{TOT}$) of a biphasic material is modeled as a function of stress strain relationship in the solid matrix ($\boldsymbol{\sigma}^{SM}$) and interstitial fluid ($\boldsymbol{\sigma}^{F}$). From Cohen et al (1998) [121].

$$\boldsymbol{\sigma}^{SM} = \phi^{s} p\mathbf{I} + \boldsymbol{\sigma}^{E} \tag{4.1}$$

$$\boldsymbol{\sigma}^{F} = \phi^{f} p\mathbf{I} \tag{4.2}$$

$$\boldsymbol{\sigma}^{TOT} = \boldsymbol{\sigma}^{E} + p\mathbf{I} \tag{4.3}$$

where pressure is p, $\mathbf{I}$ is the identity matrix, $\phi^{s}$and ϕ^{f} are the volume fraction of the solid and fluid phases respectively. The fluid phase is inviscid while the solid phase is linear elastic transversely isotropic defined by the fourth order stress tensor $\boldsymbol{\sigma}^{E} = \boldsymbol{C}\varepsilon$ based on the formulation of Cohen et al. (1998)[121]. In cylindrical coordinates the axis of transverse isotropy for the porcine corneal stroma is the z direction as reported by previous work by Hayes et al. (2007)[73] where circumferential collagen fibrillar arrangement were observed in porcine corneas. Tensile tests conducted by Elsheikh et al. (2009)[65] on porcine corneal strips of varying orientation also verified the findings of planar isotropy. A transversely isotropic stiffness tensor $\boldsymbol{C}_{ij}$ can be expressed as a function of five independent constants; the in-plane Young's modulus $\boldsymbol{E}_{r}$ $(\boldsymbol{E}_{r} = \boldsymbol{E}_{\theta})$, and Poisson's ratio $\upsilon_{r\theta}(\upsilon_{r\theta} = \upsilon_{\theta r})$, as well as the out of plane Young's modulus $\boldsymbol{E}_{z}$, Poisson's ratio υ_{zr}, and shear modulus $\boldsymbol{G}_{zr}$. The loading conditions of unconfined compression dictate that shear modulus is inapplicable in the current configuration. The continuity equation is expressed as $\nabla \cdot \left(\phi^{s}\boldsymbol{V}^{s} + \phi^{f}\boldsymbol{V}^{f}\right) = 0$, where $\boldsymbol{V}^{s}$ and $\boldsymbol{V}^{f}$ are the velocities for the solid and fluid phases. When

the inertia effects are neglected the resultant momentum relationship for the solid phase, fluid phase and total stress are given as

$$\phi^s \nabla p + \nabla \cdot \boldsymbol{\sigma}^E + \kappa_r^{-1} \left[\left(\phi^f\right)^2 \phi^s \boldsymbol{V}^s + \left(\phi^f\right)^3 \boldsymbol{V}^f \right] = 0 \tag{4.4}$$

$$\phi^f \nabla p - \kappa_r^{-1} \left[\left(\phi^f\right)^2 \phi^s \boldsymbol{V}^s + \left(\phi^f\right)^3 \boldsymbol{V}^f \right] = 0 \tag{4.5}$$

$$\nabla \cdot \boldsymbol{\sigma}^T = 0. \tag{4.6}$$

where κ_r is the radial permeability attained from the diffusive drag coefficient of relative motion. The viscoelastic response of a hydrated soft tissue in a biphasic model is hence governed by relative velocity of the solid and fluid phase that occurs when distortion to the tissue induces fluid flow and solid deformation.

In the unconfined compression configuration used in chapter 3, corneal stroma is compressed between two impermeable platens, the coefficient of friction between impermeable platens and tissue surface is assumed to be negligible[119]; this assumption results in homogeneous deformation in the z-axis during unconfined compression hence displacement in the z-axis is a function of thickness and applied experimental strain. Extrusion or imbibition of fluid is permitted freely across the cylindrical boundary surface of the corneal stroma due to the lack of radial constrains on the cylindrical boundary. The solid matrix strain tensor is expressed as a function of radial displacements u_r, and axial displacements u_z. Due to symmetry, pressure and displacement fields are axis symmetric in unconfined compression hence $\frac{\partial}{\partial \theta} = 0$ and $u_\theta = 0$. The assumption of negligible coefficient of friction between the impermeable platens and the tissue surface results in homogeneous compressive strain in the axial direction hence $u_z = z\epsilon(t)$ where $\epsilon(t)$ is the experimentally applied strain. The resultant strains are expressed as

$$\varepsilon_{ij} = \begin{bmatrix} \frac{\partial u_r}{\partial r} & 0 & 0 \\ 0 & \frac{u_r}{r} & 0 \\ 0 & 0 & \frac{\partial u_z}{\partial z} \end{bmatrix} \tag{4.7}$$

where $\varepsilon_{zz} = \frac{\partial u_z}{\partial z} = \epsilon(t)$. Previous work by Armstrong et al.[118] provided a single governing equation for radial displacements and experimentally applied strain history as

$$\frac{\partial^2 u_r}{\partial r^2} + \frac{1}{r}\frac{\partial u_r}{\partial r} - \frac{u_r}{r^2} - \frac{1}{\kappa_r \boldsymbol{C}_{11}}\frac{\partial u_r}{\partial t} = \frac{0.5r}{\kappa_r \boldsymbol{C}_{11}}\frac{\partial \epsilon(t)}{\partial t} \tag{4.8}$$

The boundary conditions for unconfined compression indicates that at the cylindrical boundary surface ($r = a$), the radial stresses $\boldsymbol{\sigma}_r = 0$ and fluid pressure $p = 0$. The resultant stress at the compressive platens can be expressed as

$$\sigma(t) = \frac{2\pi}{A_s}\int_0^a \left(-p + \boldsymbol{C}_{13}\left(\frac{\partial u_r}{\partial r} - \frac{u_r}{r}\right) + \boldsymbol{C}_{33}\epsilon(t)\right) r\partial r \tag{4.9}$$

where A_s is the area of the cylindrical sample. Cohen et al[121] provided a closed form solution to the resultant stresses acting on the platen during ramp displacement with a constant strain rate $\dot{\epsilon}_0$ as

$$\sigma(t) = \boldsymbol{E}_z \dot{\epsilon}_0 t + \boldsymbol{E}_r \frac{\dot{\epsilon}_0 a^2}{\kappa_r \boldsymbol{C}_{11}} B_3 \left[\frac{1}{8} - \sum_{n=1}^{\infty} \frac{e^{(-x_n^2 \kappa_r \boldsymbol{C}_{11} t a^{-2})}}{x_n^2 [B_2^2 x_n^2 - B_1 (1 + \upsilon_{r\theta})^{-1}]}\right] \tag{4.10}$$

The applied strain history during ramp compression ($0 \le t \le t_0$) is expressed as $\epsilon(t) = \dot{\epsilon}_0 t$. And the applied strain history during stress relaxation ($t_0 \le t \le \infty$), is constant hence $\epsilon(t) = \dot{\epsilon}_0 t_0$. The resultant stresses acting on the platen is expressed as

$$\sigma(t) = \boldsymbol{E}_z \dot{\epsilon}_0 t - \boldsymbol{E}_r \frac{\dot{\epsilon}_0 a^2}{\kappa_r \boldsymbol{C}_{11}} B_3 \left[\sum_{n=1}^{\infty} \frac{e^{(-x_n^2 \kappa_r \boldsymbol{C}_{11} t a^{-2})} - e^{(-x_n^2 \kappa_r \boldsymbol{C}_{11} [t - t_0] a^{-2})}}{x_n^2 [B_2^2 x_n^2 - B_1 (1 + \upsilon_{r\theta})^{-1}]}\right] \tag{4.11}$$

Parameters $B_1, B_2, B_3, \boldsymbol{C}_{11}$, and x_n are functions of the Young's modulus and Poisson's ratio in the out of plane and in plane directions expressed as

$$B_1 = 1 - \upsilon_{r\theta} - 2\nu_{zr}^2 \boldsymbol{E}_r \boldsymbol{E}_z^{-1} \tag{4.12}$$

$$B_2 = (1 - \nu_{zr}^2 \boldsymbol{E}_r \boldsymbol{E}_z^{-1})[1 + \upsilon_{r\theta}]^{-1} \tag{4.13}$$

$$B_3 = [1 - 2\nu_{zr}^2 \boldsymbol{E}_r \boldsymbol{E}_z^{-1}] B_2 B_1^{-1} \tag{4.14}$$

$$\boldsymbol{C}_{11} = \boldsymbol{E}_r (1 - \upsilon_{zr} \boldsymbol{E}_r \boldsymbol{E}_z^{-1})[(1 + \upsilon_{r\theta}) B_1]^{-1} \tag{4.15}$$

Parameter x_n are the characteristic roots of the Bessel equation given in equation 4.16; where $J_1$and J_0 are Bessel functions of the first kind.

$$J_1(x) - \left[\frac{1 - \nu_{zr}^2 \boldsymbol{E}_r \boldsymbol{E}_z^{-1}}{1 - \upsilon_{r\theta} - 2\nu_{zr}^2 \boldsymbol{E}_r \boldsymbol{E}_z^{-1}}\right] x J_0(x) = 0 \tag{4.16}$$

Transient stress attained from unconfined compression was curve fitted to above the closed form solution to find the fitting parameters. The Poisson's ratio for the in-plane direction $\upsilon_{r\theta}$ was assumed as 0.49, this assumption is commonly used in numerical simulations of corneal mechanics[105, 124, 143, 144]. The out-of-plane Poisson's ratio υ_{zr} was assumed as zero. Parameters $\boldsymbol{E}_r$ and κ_r were attained from the curve fitting procedure; while $\boldsymbol{E}_z$ was attained directly from the experimental result. Curve fits used to attain the theoretical predictions of $\boldsymbol{E}_r$ and κ_r were assessed based on the coefficient of determination r^2 between the transversely isotropic biphasic model and the attained experimental results.

4.4 Model prediction

The transient stress attained from unconfined compression of physiological thickness (normal) and swollen corneas after the application of 4% strain at varying displacement rates proceeded by

stress relaxation are fitted to the transversely isotropic biphasic model. Normal corneas at physiological thickness were attained from experiments conducted with a pre-stress of 7.2±0.5 KPa which is in the range of residual swelling pressures applied *in vivo* by the epithelial and endothelial pump transport mechanisms. Lower pre-stress of 1.9±0.18 KPa was applied to attain corneas swollen above its physiological thickness.

The coefficient of fit attained for average experimental stress response conducted using speeds of 0.15 μm/s, 0.5 μm/s and 1 μm/s are 0.978±0.005, 0.975±0.005, and 0.974±0.003 respectively (see. fig. 4.1). This indicates displacement rate did not affect the fitting capabilities of the transversely isotropic model to the experimental data.

The predicted elastic tensile modulus $\boldsymbol{E}_r$ was higher for normal corneas in comparison to swollen corneas; in addition $\boldsymbol{E}_r$ was amplified with increasing displacement rate. The average value of $\boldsymbol{E}_r$ predicted with increasing displacement rate are 2.10±1.14 MPa, 3.40±0.75 MPa and 3.81±1.12 MPa for normal corneas in the range of physiological thickness. For swollen corneas tested at tare stress of 1.9±0.18 KPa the resultant values of $\boldsymbol{E}_r$ are 1.36±0.21 MPa, 2.06±0.48 MPa, and 2.27±0.49 MPa at 0.15 μm/s, 0.5 μm/s and 1 μm/s respectively.

The predicted radial permeability κ_r was observed to be lower for swollen corneas in comparison to corneas in the range of physiological thicknesses. At physiological thickness, the effect of displacement rate on κ_r is observed to be independent however a more pronounced effect is observed for swollen corneas where slight increase in permeability was observed with increasing displacement rates. For swollen corneas, average values of κ_r attained at 0.15 μm/s, 0.5 μm/s and 1 μm/s are 20.6±2.5×10^{-15} m^4/N.s, 27.0±3.0×10^{-15} m^4/N.s and 30.8±0.2×10^{-15} m^4/N.s respectively. Radial permeability was observed to decrease with dehydration where average values attained with increasing displacement rates are 5.8±0.4×10^{-15} m^4/N.s, 6.1±0.2×10^{-15} m^4/N.s, and 5.9±0.4×10^{-15} m^4/N.s for normal corneas at physiological thickness.

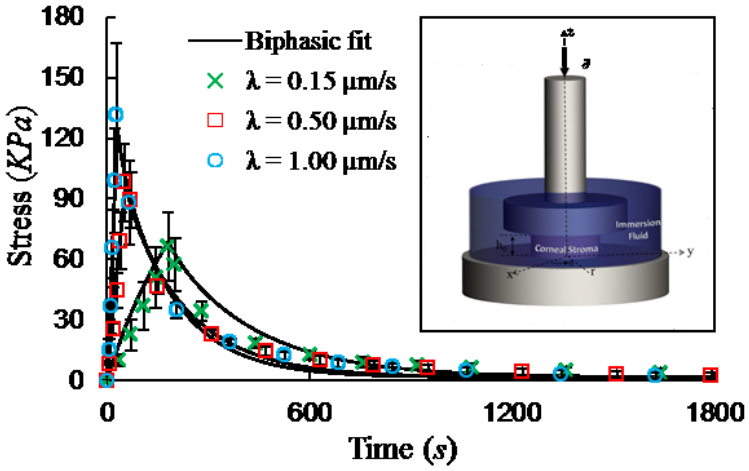

Figure 4.1: Transversely isotropic biphasic curve fit to the average transient stress attained at varying displacement rates from corneas of physiological thickness. Insert displays a schematic of the experimental setup with cylindrical co-ordinates as used in the transversely isotropic model. Error bar indicate ±1 standard deviation.

In addition to single compressive ramp and stress relaxation, experiments involving multiple compressive and stress relaxation increments from 4-50% strain were also modeled to determine transient consolidation properties of the cornea based on experimental observations from tests conducted using varying displacement rates and temperature.

It was observed that the transversely isotropic biphasic model was able to fit the transient experimental stress data from 4% to 50% incremental stress strain compression, for the three displacement rates applied during experimentation at a constant temperature of 37° C. The model fit to the average transient stress attained from the compressive displacement rate of 0.15 µm/s is given in figure 4.2. An incremental increase in compressive strain was observed to increase $\boldsymbol{E}_r$ linearly up to 20% strain after which non-linear increase was observed while κ_r decreases exponentially from 4-50% strain. The average predicted values of $\boldsymbol{E}_r$ and κ_r are presented in figure 4.3-4.4; where the effects of displacement rate are presented. The average predicted values

for $\boldsymbol{E}_r$ are observed to increase with increasing compressive strain. Furthermore increase in displacement rate was also observed to amplify its value. Slight increase in $\boldsymbol{E}_r$ was observed when fresh samples were compared to freeze-thaw samples, nevertheless this variation was not significant across all strains. It is observed that $\boldsymbol{E}_r$ displays temperature independent behavior between 25°C to 40°C. For instance, at constant strain (50%) and displacement (0.15 μm/s), the average values for $\boldsymbol{E}_r$ are 5.8 MPa, 6.4 MPa and 4.8 MPa for 4°C, 25°C, 37°C and 40°C respectively. When sample diameter was reduced to 8 mm, $\boldsymbol{E}_r$ was observed to be independent of sample diameter across all strain increments. At 50% strain, the average values for $\boldsymbol{E}_r$ are 5.8 MPa, and 6.4 MPa for 8mm and 10 mm diameter samples respectively.

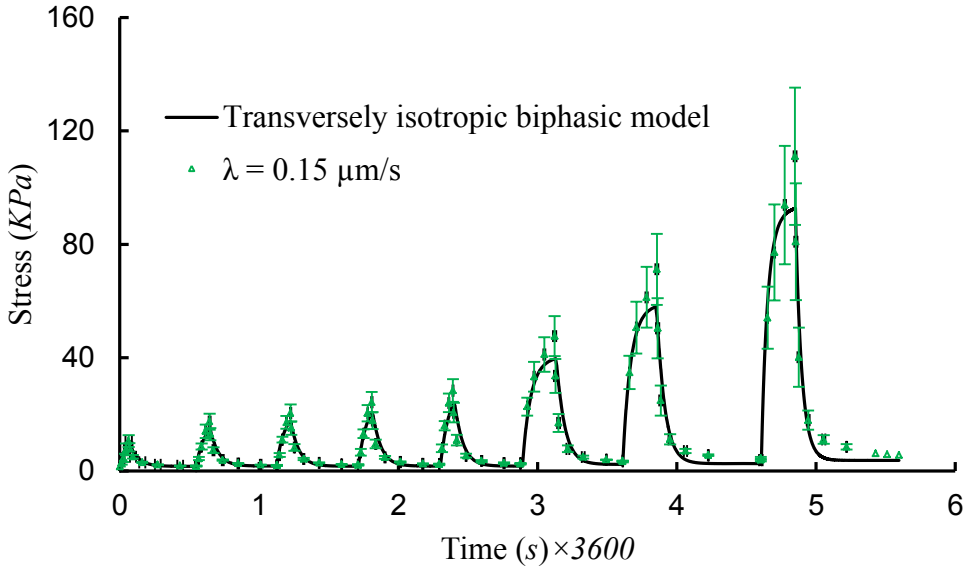

Figure 4.2: Transient fit of the transversely isotropic biphasic model (black line) to average stress observed in unconfined compression experiments (green triangle) conducted at displacement rate of 0.15μm/s from 0% to 50% strain.

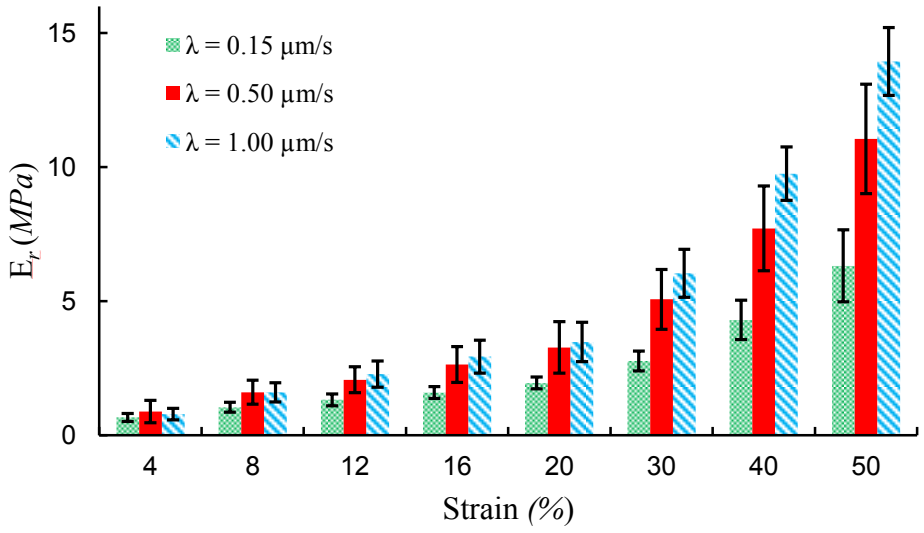

Figure 4.3: The variation of in-plane modulus ($\boldsymbol{E_r}$) with displacement rate

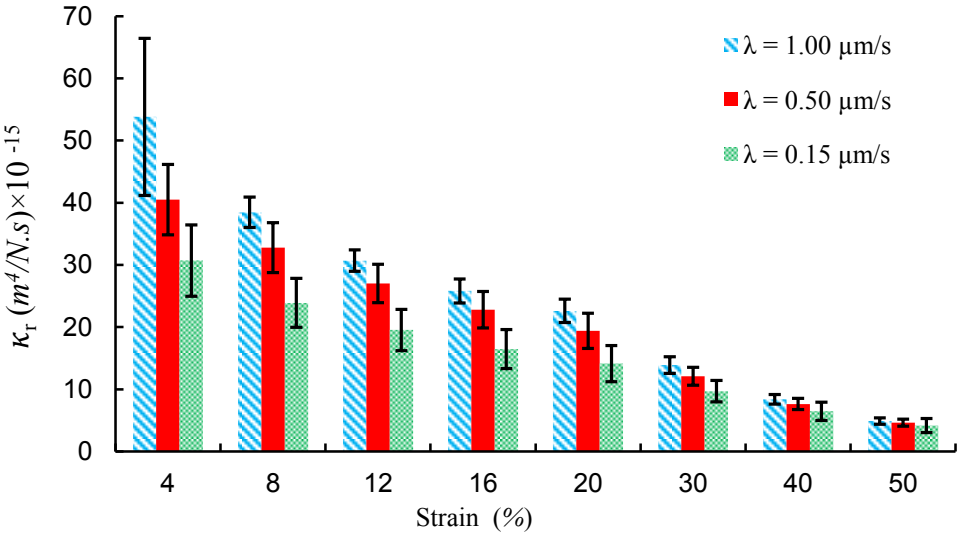

Figure 4.4: The variation of radial permeability (κ_r) with displacement rate.

The predicted values for κ_r is observed to display dependence on displacement rate especially at low strain levels, decrease in temperature is also observed to reduce κ_r at strains greater than 8% where this effect is observed to be more pronounced at higher strains. No statistical difference

was observed for κ_r attained from fresh and freeze-thaw samples. At 50% strain, the average values of κ_r are 4.3×10^{-15} m^4/N.s, 4.1×10^{-15} m^4/N.s, and 2.3×10^{-15} m^4/N.s, for 40°C, 37°C, and 25°C respectively. No difference in κ_r is observed from samples of 8 mm and 10 mm diameter.

The experimental transient stress behavior of the corneal stroma attained from unconfined compression was modeled using a transversely isotropic biphasic model. This model accounts for the solid and fluid interactions in the stroma as well as anisotropy. Analytical solution of the transversely isotropic model was curve fitted to the experimental data to attain elastic tensile modulus and permeability where the model was able to properly fit the experimental data based on the goodness of fit. The predicted elastic tensile modulus was observed to increase with displacement rate for normal and swollen corneas, this rate dependent behavior for tensile modulus has previously been observed in uniaxial tensile tests of corneal stroma. In addition, elastic tensile modulus was observed to increase with increasing compressive strain; this is also in correlation with previous reports where corneal Young's modulus increased with decreasing thickness/hydration. The ranges of predicted tensile modulus are within the rages of values attained from uniaxial tensile stress relaxation test by Pandolfi et al. (2012) as 2.5 to 17.5 MPa[103]. At low compressive strains an average of 0.6 MPa is observed , this value increases on average to within 2.6 to 3.8 MPa at physiological thickness based on the applied displacement rate. At high compressive strains tensile modulus of 13 to 14 MPa was also predicted. Although, the lower range of predicted elastic tensile modulus is below the reported range, it should be noted that Young's modulus of 0.4 MPa were reported from static tensile tests[65, 145], thus the lower range of elastic tensile modulus could coincide with stress levels below the minimum range of stresses tested by Pandolfi et al (2012).

Radial permeability was observed to decrease with compressive strain and corneal detergence; this is in correlation with previous reports by Hedbys et al. (1962)[146] Furthermore as compressive strain exceeds 12%, an increase in temperature is observed to decrease permeability. The increase

in corneal permeability with increasing temperature was also reported by Fatt (1971)[90] and Hedbys et al (1963)[147]. At physiological thickness/hydration, the average radial permeability predicted in this study at 25°C is 2.3×10^{-15} m^4/N.s. This is similar to values reported by Hedbys et al. (1962) as 1.5×10^{-15} m^4/N.s at physiological thickness/hydration[146]. Further comparison of predicted radial permeability and the experimentally reported permeability displays a deviation in predicted and experimental values as experimental lay attained permeability are lower than the predicted radial permeability. It should also be noted that experimentally attained permeability was attained from the axial direction; Hedbys et al. (1962) reported the radial permeability to be more dependent on thickness/hydration in comparisons to the axial direction however they were not significantly different at physiological thickness/hydration. Additional reports on corneal permeability by Stewart et al (2009) reported porcine corneal permeability of $82\pm15\times10^{-15}$ m^4/N.s at temperature 37°C where corneal thickness was 1.02 mm[148], within that range the average radial permeability is between $19\text{-}27\times10^{-15}$ m^4/N.s. Corneal flow velocity K attained from topical drug delivery studies can also be used to attain permeability as $K = \rho g \kappa_r \mu^{-1}$ where density ($\rho = 999$ kg/m^3)[149], and dynamic viscosity ($\mu = 0.7$ mPa.s)[150] of 0.9% NaCl at 37°C and gravity g are used in the calculation. The reported values of flow velocity range from $2.5\text{-}9.89\times10^{-5}$ cm/s[151], this corresponds to permeability in the range of $1.7\text{-}7.1\times10^{-15}$ m^4/N.s which is in agreement with the predicted permeability attained in the current study.

4.5 Finite element implementation

When sample geometry vary from the axisymmetric geometries, the analytical solution for the transversely isotropic biphasic model turn out to be complex thus numerical finite element method is implemented to solve such computational mechanics problems. FEBio[152] is an open source finite element program that offers orthotropic biphasic model that can be used to approximate the displacement, fluid pressure, stresses and strains using the virtual work equation. FEBio was used to model the cornea in unconfined compression, and the numerical solution was compared to the analytical closed form solution.

Quarter symmetry cylindrical sample was modeled in the current study where radius and height of the cylinder were 5 mm and 0.698 mm respectively. Sample height was based on the average height of corneas after tare stress of 7.2±0.5 KPa (See chapter 3). Boundary conditions due to quarter symmetry results in fixed displacement in the X and Y direction for nodes in the Y-Z plane and X-Z plane respectively.

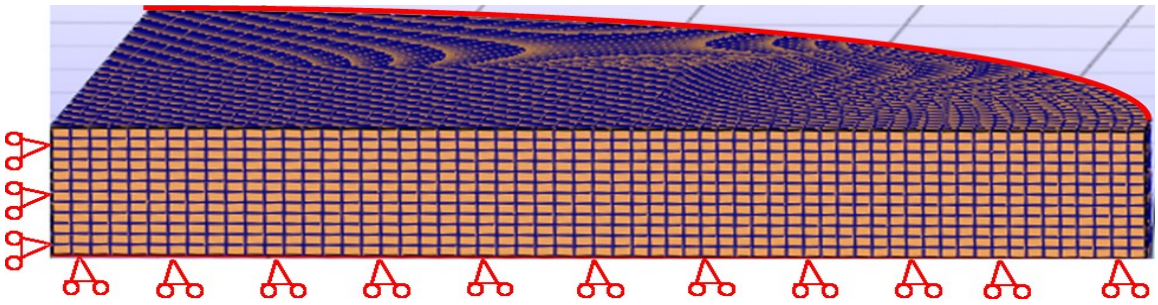

Figure 4.5: Boundary Conditions of quarter symmetry cylindrical mesh. Fluid pressure is set to zero for nodes at the radial edge of the cylinder.

Additional boundary conditions from unconfined compression experiment were implemented by setting zero fluid pressure at the radial surface for fluid flow through the radial boundary, fixed displacement for nodes at the bottom of the Z plane and prescribed displacement for nodes at the top of the Z plane. A prescribed displacement of 0.0279 mm in 30.2 seconds was implemented

followed by constant displacement for 1500 seconds. Material properties $\boldsymbol{E}_r$ and κ_r attained from the analytical curve fit, and $\boldsymbol{E}_z$ from unconfined compression experiments conducted at 1μm/s as given in section 4.4.

Hexahedral mesh was implemented with 8 node hexahedral elements with a butterfly center of two different densities. Two mesh densities were generated to determine the effect of mesh density on the convergence to the experimental data and closed form solution. Lower density mesh possessed 11, 349 nodes and 9,600 elements in 20 by 20 by 8 divisions in the X, Y and Z axis. High density mesh had 36,283 nodes, 32,400 elements in 30 by 30 by 12 divisions in X, Y and Z axis. Biphasic solver analysis was implemented using a step size of 0.1, and 40 optimal quasi-Newton iterations.

It is observed that the numerical solution for transient stress attained from FEBio using the low density mesh does not converge to the close form solution; nevertheless the results attained high density mesh is in agreement with the analytical solution as well as the experimental observation. A comparison of the fluid pressure attained numerically also converges to the closed form solution of the transversely isotropic model. The predicted transient radial displacement from the FEA model displays shrinkage in sample diameter during stress relaxation however this cannot be verified as radial displacement was not monitored during experimentation.

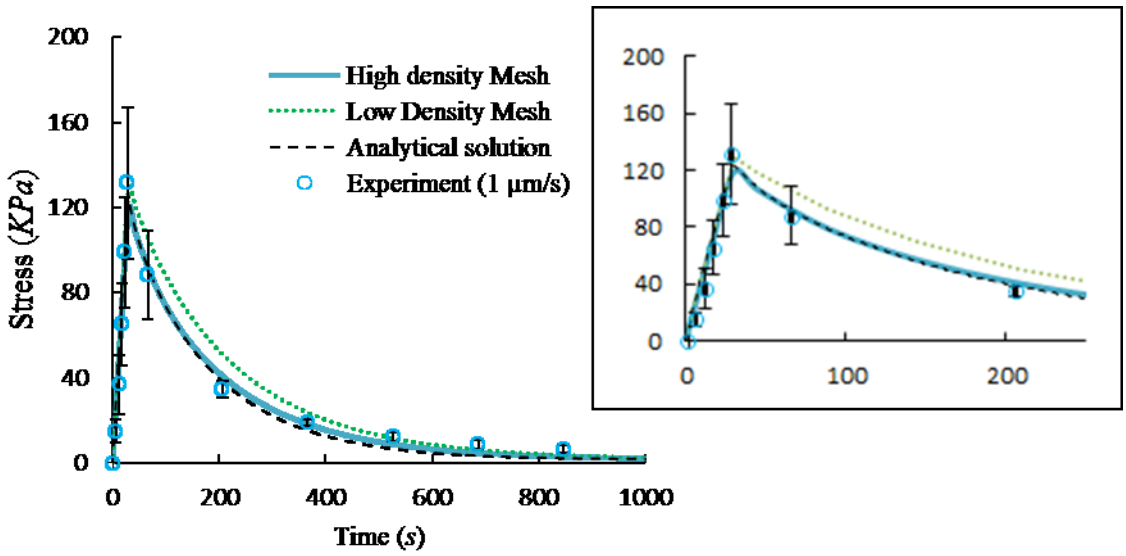

Figure 4.6: A comparison of the numerical solution attained from low and high mesh density for the transient stress behavior from unconfined compression. The high density mesh converges to the analytical closed form solution. Data not shown past 1000 seconds due to convergence. Insert shows analytical and numerical fit in the ramp and early stress relaxation for clarity.

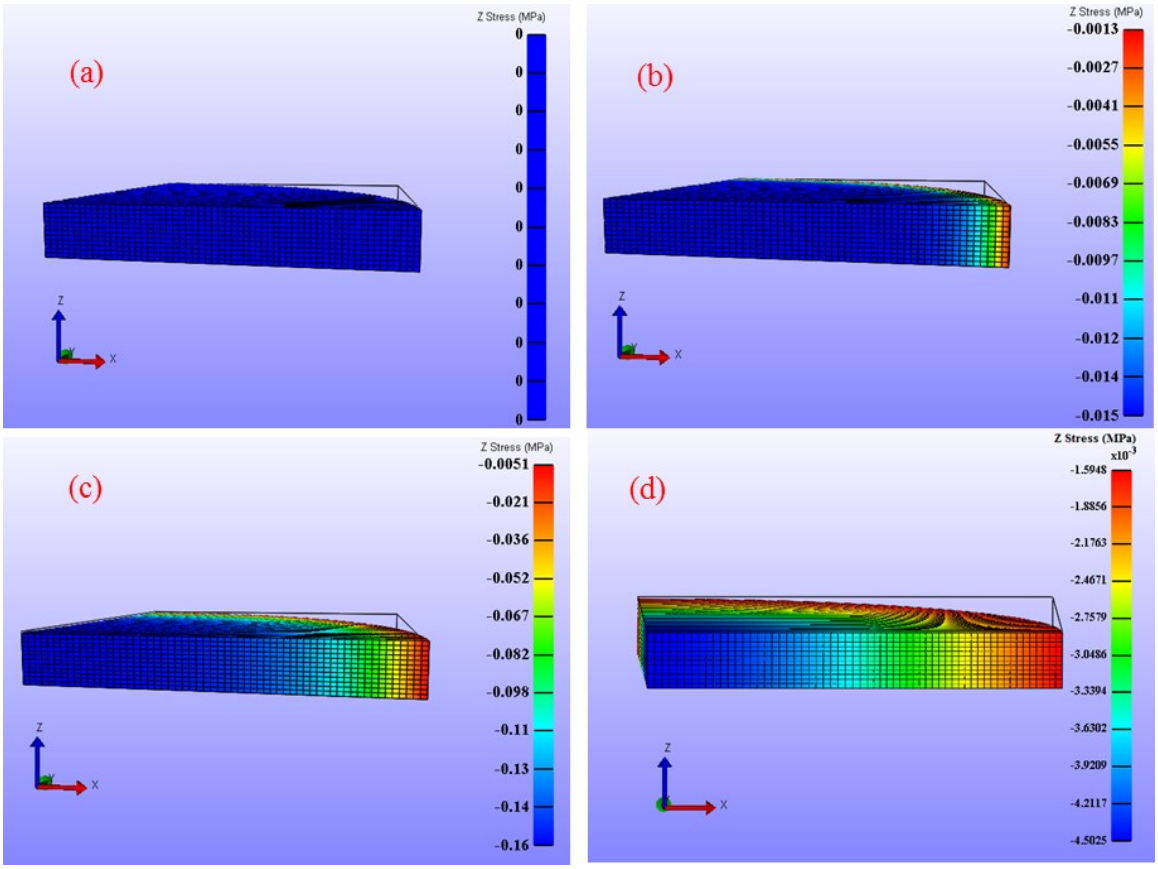

Figure 4.7: The distribution of stresses predicted by the numerical solution at (a) time = 0 where prior to compression (b) time = 3 seconds where stresses at the radial boundary are less than stresses at the interior (c) time = 30 seconds; at peak compressive strain where radial displacement is maximum (d) time =1000 seconds; contraction of radial displacement as well as convergence of stress dissipation. It should be noted that the color map displays stresses in term of compression thus colors at the bottom of the map indicate levels of higher compressive stresses. Solid wire box indicates the external bounds of the quarter cylinder prior to compression.

Application of the transversely isotropic biphasic model to finite element analysis produced transient stress solution that converged to the experimental transient stress as well as the analytical solution. This numerical model provides the ability to display transient inhomogeneous depth dependent axial and radial displacement, as well as the variation of stress and fluid pressure in the radial direction. Validation of the predicted inhomogeneous radial and axial displacements could be attained using digital imaging correlation during unconfined compression as performed by Gao et al (2012)[153] where transient imaging and digital imaging correlation were implemented

to determine local strains though the thickness of cartilage specimens in addition to the macro deformation measured from platen to platen.

Limitations of the transversely isotropic model include the assumption of linearity as the cornea displays nonlinearity in tis stress-strain behavior in a variety of loading conditions. The inability to explicitly model anisotropic collagen fibrils is also a limitation as transversely isotropic fibrillar distribution is limited to species of which corneal stromas was attained. In addition, the effect of ionic concentration is not explicitly modeled as the effect of Donnan osmosis is lumped into the compressive modulus. In the curve fitting procedure, values for parameters $\boldsymbol{E}_r$ and κ_r were attained based on the highest value for the goodness of fit, the uniqueness of the parameters attained by maximizing the goodness of fit were not analyzed. Nevertheless, the predicted values for $\boldsymbol{E}_r$ and κ_r were in the range of previously reported values. In addition, the decrease in κ_r and increase in $\boldsymbol{E}_r$ with decreasing hydration predicted by maximizing the goodness of fit was also in correlation with their experimentally observed behavior. Further limitations rise from the absence of intrinsic viscoelasticity in the transversely isotropic biphasic model. This omission can also be seen in the prediction of peak stress attained at high displacement rates.

CHAPTER V

VISCOELASTIC SHEAR PROPERTIES OF THE CORNEA

5.1 Introduction

Quantification of corneal viscoelastic behavior is of essence in the development of realistic analytical and numerical models for corneal mechanics that can provide support to refractive surgical procedures. The ability to accurately predict corneal deformation caused by surgical incisions or laser ablation enables the surgeon to attain the desired shape of the post-operative cornea required for refractive correction of vision. Application of numerical models to simulate corneal mechanical behavior has generated significant interest; numerical model based on the combination of isotropic, and anisotropic hyperelastic deviatoric strain energy formulations have been applied to numerical surgery simulations[126, 154]. The isotropic strain energy function characterizes the corneal matrix and it is generally a function of shear modulus, a material parameter that can be quantified experimentally by testing the cornea under shear loads.

The cornea is reported to display rate dependent and time dependent viscoelasticity, where nonlinear viscoelasticity was also observed at non-physiological stresses. However most of these viscoelastic properties were attained from static testing configurations under tensile or compressive loads. Dynamic loads are applied to the cornea from contraction and relaxation of ocular muscle fibers, as well as the applanation of external objects such as surgical instruments that subjects the cornea to shear loads. Initial dynamic shear studies by Soergel et al. (1995)[114]

reported corneal shear compliance to vary with corneal thickness, port mortem interval, experimental temperature at a constant frequency. In addition the variation in frequency at constant thickness or temperature was also observed to affect the measured shear compliance. Recently oscillatory stress or strain controlled rheometer were employed to characterize corneal shear modulus. Nickerson (2006)[115] reported the storage modulus of the cornea at varying oscillatory strains at a constant frequency in addition to the effect of glyceraldehyde corneal stiffening on storage modulus of the cornea at constant strain and frequency. Petsche et al. (2012)[1] studied the variation of storage modulus with varying compressive strains on whole corneas and corneal flaps attained from anterior, middle and posterior corneal section where storage modulus was observed to increase with an absolute increasing compressive strain or stress. Although these studies have highlighted the variation of corneal viscoelastic properties in shear, no information was provided on the limit of linear viscoelasticity, shear stress relaxation behavior, and the effect of strain rate on the transient shear stress or shear stress strain behavior. Thus it is the aim of this chapter to experimentally characterize shear viscoelastic properties of the cornea using a rheometer. Due to the lack of time, the data presented in this chapter was obtained from a limited number of experiments and should only be regarded as preliminary results. Future careful studies are required for full characterization of the corneal shear properties.

5.2 Materials and Methods

5.2.1 Sample preparation

Enucleated porcine eye globes were attained from a local slaughterhouse and transported to the laboratory on ice. The corneas were observed for edema and scratches after which corneas free from scratches and edema were enucleated in a similar manner as described in chapter 2 thus a brief description is given here. A dulled edge Scalpel was used to debride the corneas epithelium,

then an incision was made at the corneo-scleral junction with the scalpel. Scissors were inserted in the incision, and a circular cut was made around the sclera to excise the cornea with a scleral rim. The endothelial layer was rubbed off using Kim wipes and a trephine was used to attain 8 mm or 6 mm cylindrical stromas from the central region of the cornea.

5.2.2 Test Protocol

Measurements of corneal shear viscoelastic properties were conducted using a DHR 2 rheometer (TA Instruments, Delaware) with a minimum torque oscillation of 2 nN.m, torque resolution of 0.1 nN.m, minimum frequency of 10^{-7} Hz, and displacement resolution of 10 nrad. Thermal controlled submersion kit was used to implement an experimental temperature of 25±0.1°C for all experiments. TRIOS software (TA Instruments, Delaware) was used to record the experimental torque, normal force and displacement as well as calculate stress, strain, dynamic and time dependent viscoelastic properties. To prevent sample dehydration experiments were conducted in submerged conditions where OBSS was employed as the submersion fluid. Prior to mechanical testing, samples were immersed in OBSS for 30 minutes to equilibrate. Shear displacement was applied to the trephined corneal samples by 8 mm upper parallel plate geometry in a plate to plate centered configuration. Shear stress τ and shear strain γ were calculated as a function of torque T and radius of parallel plate R, angular displacement θ and height of sample H_i as shown in figure 5.1.

$$\tau = \frac{2T}{\pi R^3} \tag{5.1}$$

$$\gamma = \theta \frac{R}{H_i} \tag{5.2}$$

In the linear viscoelastic region, when sinusoidal displacement amplitude of θ_0 is applied at a given frequency ω, a torque response is generated which is a function of the torque amplitude T_0 and phase shift angle δ.

$$G' = \frac{2T_0H_i}{\pi R^4}\cos(\delta) \tag{5.3}$$

$$G'' = \frac{2T_0H_i}{\pi R^4}\sin(\delta) \tag{5.4}$$

$$\delta = tan^{-1}\frac{G''}{G''} \tag{5.5}$$

$$G(t) = \frac{\tau(t)}{\gamma} \tag{5.6}$$

Viscoelastic material properties such as storage modulus G', loss modulus G", phase shift angle are calculated as given in equations 4.3 to 4.5. When instantaneous strain is applied and held constant over time, the stress relaxation modulus G(t) was calculated using equation 5.6.

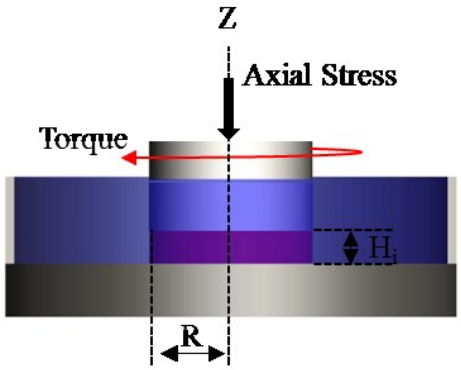

Figure 5.1: Experimental schematic displaying the multi loading conditions applied to the cornea during shear viscoelastic testing where R is the sample radius and H_i is the sample thickness.

5.2.2.1 Wall Slip

In order to attain accurate characterization of the corneas shear viscoelastic properties, no slip boundary condition is required during experimentation. This condition requires that the velocity of the upper rotating parallel plate geometry to be equal to the velocity of the cornea during shear while the velocity at the bottom surface of the cornea and lower geometry is zero in order to

measure the proper sample deformation. Sand paper is commonly glued to the top and bottom parallel plate geometries to prevent slippage when characterizing the rheological properties of soft tissues and other materials that violate the no slip boundary condition. Coarse sand paper (80-150 grit) is generally used to prevent slippage[155-158], however recent study by Petsche et al employed 320 grit fine sand paper. Furthermore, at high strain rates wall slip has been reported to occur in the presence of sand paper.

The effect of surface roughness was characterized by conducting varying oscillatory strain experiments at constant frequency and constant shear rate experiments on 8 mm corneal stromas using parallel plates with smooth surface, fine sand paper (320 grit) and coarse sand paper (80 grit). This was performed by placing corneal samples in OBSS for 30 minutes prior to mechanical testing after which corneal stroma is centered underneath the parallel plates and compressed until 0.1 N of axial force was attained after which axial displacement was kept constant for experimentation.

Visualization technique was employed to determine when no-slip boundary condition was violated by drawing a parallel vertical line with a water proof marker from the upper parallel plate through the radial sample surface to the lower surface of the parallel plate geometry. Continuous marks between the parallel plates and the radial surface of the corneal stroma indicates no-slip boundary condition was upheld. Due to the use of visualization technique, a submersion chamber was not used in this test instead 3ml of OBSS was used due to the short experimental duration. This was done by pipetting OBSS on the bottom sandpaper in a manner that the radial corneal surface was engulfed by OBSS. Preconditioning was implemented to attain a reference experimental state for corneal stromas by applying constant oscillatory shear strain and frequency of 0.2% and 1 Hz respectively; where the attained storage modulus was recorded over time to determine if steady state behavior had occurred. Varying amplitude oscillation strains from 0.001 to 15% at frequency of 1 Hz were conducted after which rest period of 20 seconds was allowed

followed by constant strain at 0.5/s. Each study was conducted on parallel plates with smooth surface, fine sand paper and coarse sand paper.

5.2.2.2 Validation of shear testing technique

There are two previous reports of corneal storage modulus in the literature. In order to validate the experimental studies of this chapter, 8 mm and 6 mm corneal stromas were tested using previously reported shear protocols.

Petsche et al. (2012), conducted oscillatory shear experiments on 6 mm diameter Human corneas of full thickness corneal stromas previously stored in Optisol storage medium, a rheometer with 320 grit sand paper was used to apply strain. Corneal stromas were compressed to a thickness 15% below the measured corneal thickness. Optisol was added to their submersion chamber after which test temperature of 37°C was set. Sinusoidal oscillatory shear loading was implemented at 1% strain at constant frequency of 0.03 Hz; this test was conducted for four cycles where the initial three cycles are preconditioning cycles after which the fourth cycle is recorded. This cycle was repeated after the implementation of 5% compressive strain using axial displacement rate of 1 μm/s after which the transient compressive strain was allowed to equilibrate for five minutes. Further compressive strain increments of 5% were implemented until 40% compressive strain was attained.

In the current study, modifications made to the current testing protocol includes the use of porcine corneas as Human corneas were unavailable, corneal storage medium was changed from Optisol to OBSS, and an increase of relaxation time from 5 minutes to 30 minutes as the transient compressive stress did not equilibrate in 5 minutes.

Furthermore, Nickerson (2006) employed an 8 mm diameter parallel plate geometer with 35-40 cleats, 0.6 mm thick to characterize porcine cornea shear modulus. Corneal stromas attained from the central region (8 mm) were compressed until 0.1 N compressive force, this force was allowed to dissipate after which oscillatory stress of 1 to 30 Pa was applied at constant frequency of 1 rad/s where vapor trap was employed to preserved hydration.

In the current study, a submersion chamber was used to preserve hydration however sample diameter, frequency, and oscillatory stress were the same as used by Nickerson.

5.2.2.3 Strain sweep test

Compressive tare stress of 6.4±0.6 KPa was applied to the cornea for 30 minutes, this tare stress was selected slightly below the range of swelling pressure range of corneal swelling pressure (6.6- 7.9 KPa). Thickness of the cornea after equilibration of the tare stress was used as the initial thickness for calculating axial compressive strains after which compressive strain of 10% was applied with a compressive speed of 1 μm/s and relaxation time of 20 minutes. The limit of linear viscoelasticity was determined by applying varying strain amplitudes from 0.01% to 10% strain at a constant of 1 Hz frequency on 8 mm corneal stromas (n=5). Based on the pre-test (see section 4.3) 4 cycles of preconditioning was applied to attain a steady state of corneal shear properties; posteriori shear properties were recorded for 3 cycles.

5.2.2.4 Stress relaxation test

Stress relaxation tests were performed after the final cycle of strain sweep test by implementing a strain rise time of 0.01 s to attain an instantaneous shear strain of 0.1%, after which this strain was held for 200 seconds. The effect of shear strain on transient corneal response was conducted by applying 3 additional levels of strain (0.2%, 5%, and 10%) where each stain level was held constant for 200 seconds. Shear strain was then reversed to zero strain level by applying incremental shear strain reversal of -5%, -4.8%, -0.2%, and -0.2% where each strain level was kept constant for 200 seconds. The transient stress and stress relaxation modulus was recorded at each shear strain increment.

5.2.2.5 Dynamic oscillatory test

Dynamic shear tests were performed following the cycle of shear stress relaxation tests (zero strain) by applying constant shear strain in the region of linear viscoelasticity using varying frequencies of 0.03-20 Hz. Conditioning interval of 4 cycles was applied for each test after which the storage modulus, and loss modulus were recorded for the next 3 cycles.

5.3 Results and Discussion.

5.3.1 Wall Slip

It was observed that the storage modulus attained using 320 grit or 80 grit sand paper did not differ at the same equilibrium stress. In the case of constant strain rate experiments where strain was implemented at 0.5/s, the stress strain behavior attained from both sand paper were within the same range as the rupture point was unaffected. Experiments conducted without sand paper failed

to comply with the no-slip boundary condition as slippage was observed visually as well as in the recorded stress-strain behavior where rupture point was not observed.

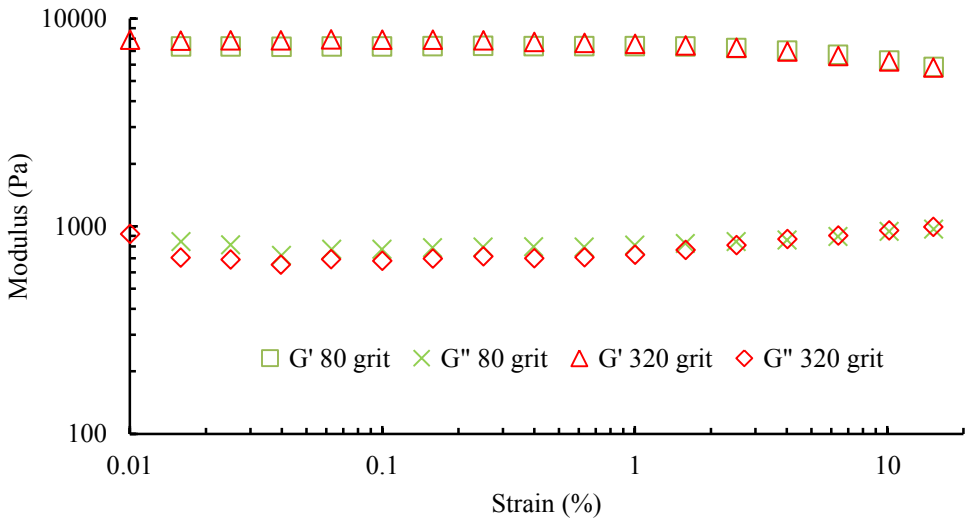

Figure 5.2: Storage modulus and loss modulus attained from corneas tested on 80 and 320 grit sand paper after the application of 0.1 N compressive force from two samples.

5.3.1 Validation of shear testing technique

Experiments conducted using the same shear testing protocol as Nickerson generated an average storage modulus in the range of 900 to 817 Pa for oscillatory shear stress varying 1 to 30 Pa, while Nickerson attained values in the range of 680 to 580 Pa as extrapolated from tests conducted with cleated geometry (See Nickerson figure 9). Although the average shear stress values from this current study are higher than previous report, they are within one standard deviation.

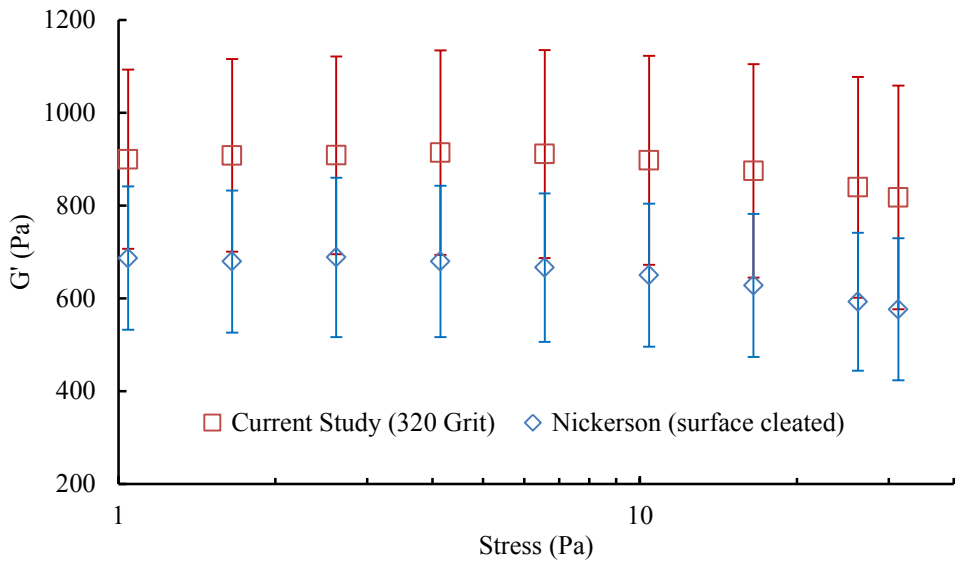

Figure 5.3: Experimental comparison of shear modulus attained from porcine corneas from current study and previous report by Nickerson[115]. Nickerson data extrapolated using optical analysis.

The variation of storage modulus attained at depth dependent equilibrium stress attained using a similar protocol by Petsche et al. generated similar shear modulus at lower equilibrium compressive stresses. At higher equilibrium shear stresses the shear modulus reported by Petsche et al was higher than the shear stresses observed in this study. Nevertheless, these values were of the same magnitude and additional difference due to species of sample could have played a role in the observed variation.

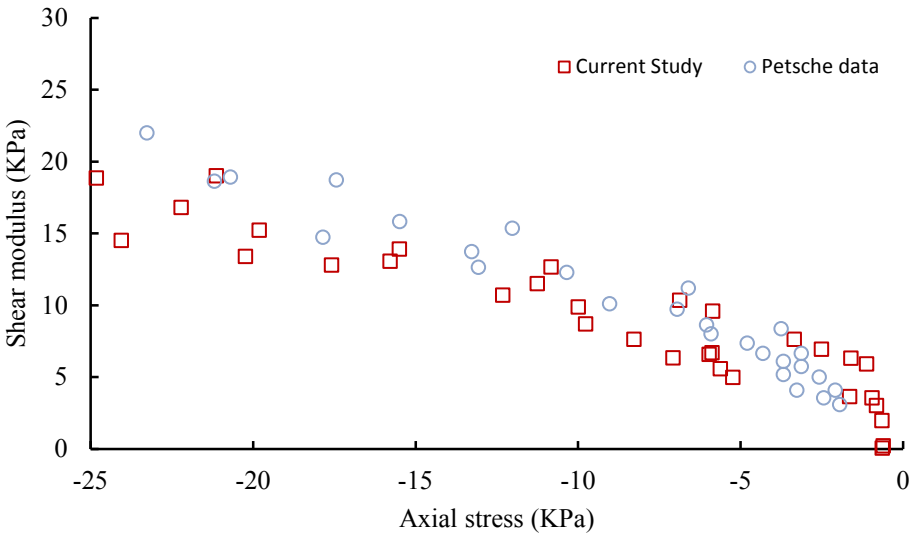

Figure 5.4: Experimental comparison of shear modulus attained from porcine corneas from current study and previous report by Petsche at al[1]. Petsche et al. data extrapolated using optical analysis.

5.3.2 Strain sweep test

It is observed that G' and G" were steady at strains below 0.3% where the average variation of G' is less than 1.7% thus corneal stroma has a linear viscoelastic limit (LVL) of 0.3%. In the LVL the average value of G' and G" were 7.1 KPa and 1.19 KPa respectively.

5.3.3 Strain sweep test

For dynamic tests conducted at constant strain of 0.3%, it is observed that an increase in frequency increased G' at all frequencies tested. It was also observed that G" was independent of frequency less than 0.3 Hz where the incremental change in G" was less than 5%. Frequencies above 0.3Hz increased the magnitude of G", a comparison of G" attained at 0.03 Hz and 20 Hz displays an increase in value by 4 to 6 times.

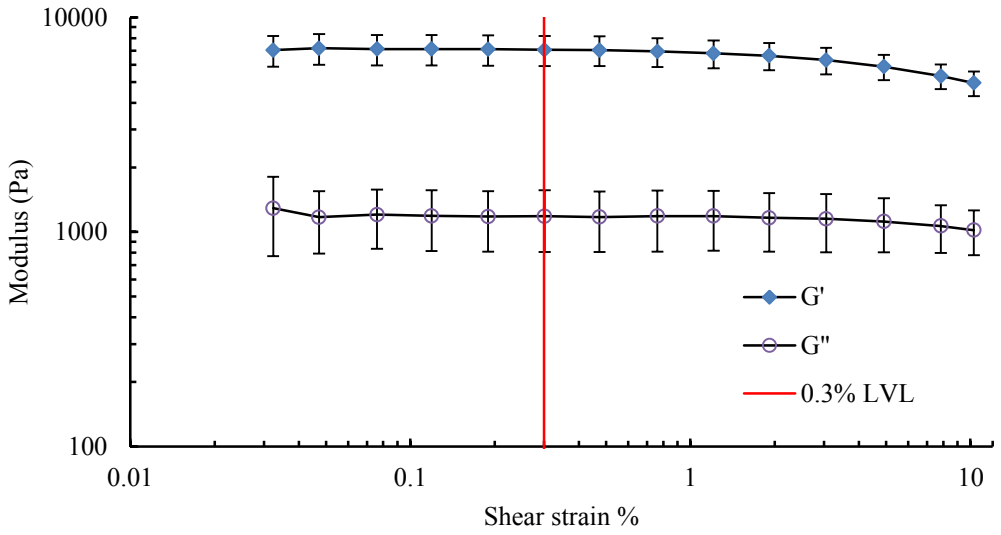

Figure 5.5: The average variation of G' and G" with increasing shear strain at 10% axial compressive strain. Linear viscoelastic limit of 0.3% is observed where G' varies by less than 1.7% on average.

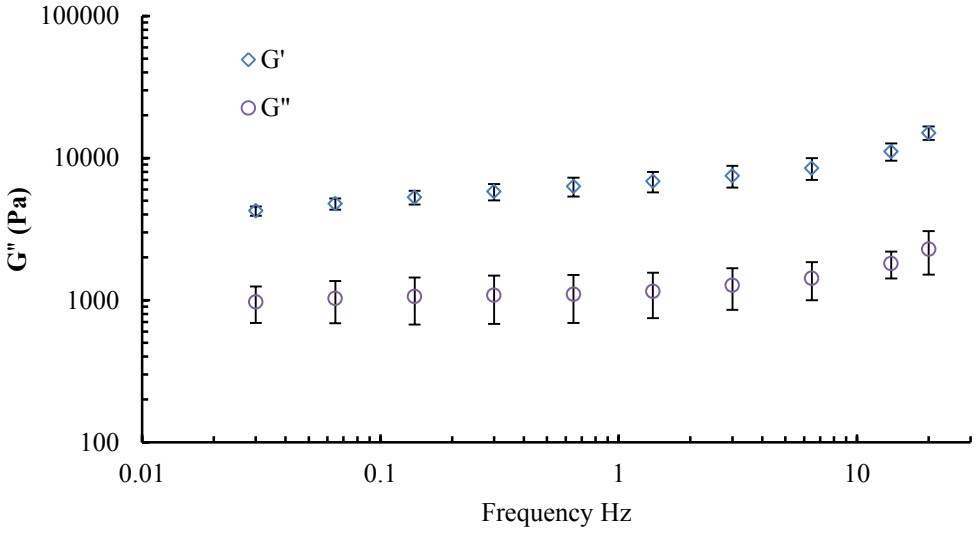

Figure 5.6: The average variation of G' with increasing frequency (0.03 Hz to 20 Hz) at 0.2% shear strain attained at compressive strains from 0% to 40%.

4.3.4 Stress Relaxation tests

It was observed that when instantaneous shear strain was applied and kept constant, the transient shear stress decreased to an equilibrium shear stress. Incremental increase of the applied instantaneous shear strain resulted in higher equilibrium shear stresses. The calculated G(t) was observed to decreases with increasing shear strain thus indicating the nonlinear viscoelastic behavior of the cornea.

The equilibrium stress attained from the shear loading and unloading behavior of the cornea displayed hysteresis as the equilibrium stress attained at the same shear strain during the loading phase was higher than the value attained while unloading shear strain.

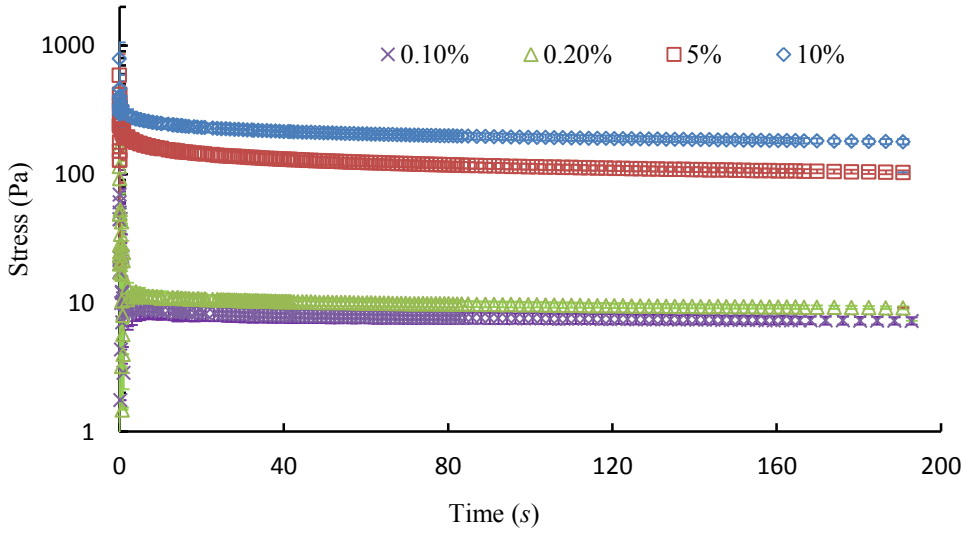

Figure 5.7: The average shear stress attained at varying incremental shear strains.

A comparison of the average equilibrium shear modulus with the equilibrium compressive modulus attained at the same strain increment indicates that at the same thickness the equilibrium compressive properties are 8 to 16 times larger than the equilibrium shear modulus.

Corneal stromas were tested in either oscillatory shear in static or dynamic frequencies, in addition to stress relaxation. Shear stress relaxation as well as oscillatory strain controlled static and dynamic frequency tests was conducted at 10% compressive strain after applying a tare stress of 6.4 KPa. During oscillatory shear tests, it was observed that G' and G" were constant for strains less than 0.3% thus indicating the corneal shear linear viscoelastic limit. In other soft tissues such as the kidney and brain, linear viscoelastic limit is observed to be within 0.1% to 1%[155, 157, 158]. As observed in previous reports by Soergel et al[114], increase in oscillation frequency or compressive strain was observed to affect the measured shear properties.

Time dependent shear properties attained from instantaneous shear strain at varying shear strain increments displayed an increase in equilibrium shear stress and decrease in G(t) which is also an indication of corneal non-linear shear-stress-strain behavior. Hysteresis loop was attained when the incremental shear strain was unloaded with a similar incremental strain used during the loading protocol.

The shear viscoelastic properties attained from this study provides experimental data that can be used in validation of mathematical models as well as reduce the number of unknowns in such numerical models. Elastic, viscous, viscoelastic, and damping parameters of the cornea can be attained based on the calculated modulus given as well as curve fitting the experimental results presented. Parameters associated with isotropic hyperelastic strain energies such as the short term time and long term time shear modulus are provided in this report at varying states of corneal thickness. Time dependent stress relaxation parameters such as the long term elastic modulus and zero shear viscosity can be attained from fitting stress relaxation data attained at 0.1% strain in

the LVL. In addition the use of reduced relaxation function that include short term τ_1 and long term τ_2 time constant as well as the dimensionless spectrum magnitude C, are related to the ratio of instantaneous to equilibrium modulus attained form purely intrinsic viscoelasticity[123]. The low shear strain amplitude applied at 0.1% stress relaxation results in only intrinsic viscoelasticity thus the ratio of instantaneous to equilibrium modulus $G(1)/G(200) = [1+c \ln(\tau_2/\tau_1)]$. Fitting data from constant shear rate tests provide damping parameters related to coefficient of viscosity, inception of nonlinearity and yield.

CHAPTER VI

CONCLUSIONS AND FUTURE RESEARCH

6.1 Conclusions

Mechanical properties of corneal stroma were studied using unconfined compression where the instantaneous, transient and equilibrium behavior of porcine corneas were characterized at varying displacement rates and compressive strains. Results from these tests indicated the instantaneous properties were dependent on displacement rate and compressive strain while the equilibrium behavior was independent of the displacement rate.

An analytical solution of the transversely isotropic biphasic model was used to analyze the transient response of the cornea in unconfined compression where tensile modulus and radial permeability were attained numerically. This model was able to fit the equilibrium stress response; nevertheless, it underestimated the peak stress especially for experiments conducted at high displacement rates. The in-lane Young's modulus, out of plane Young's modulus and permeability of the porcine cornea were estimated as a function of tissue thickness and loading rate. The predicted tensile modulus attained was within the range of reported values attained from uniaxial testing. Predicted radial permeability was slightly higher than the reported permeability of the porcine cornea.

The transversely isotropic biphasic model was also implemented in a finite element analysis. The material properties attained from the closed form solution was used to numerically simulate the

corneal behavior in the unconfined compression experiment. Transient stress attained from the finite element solution converged to the analytical solution and experimental observation. Static and dynamic oscillatory shear were performed and the linear viscoelastic limit of the corneal stroma was determined. Frequency was also observed to affect G' and G" as both values increased with increasing frequencies. The application of instantaneous strains followed by constant strain period revealed the dissipation of stress with time until stress approached an equilibrium stress. Further increase in shear strain increased the equilibrium shear stress value. Hysteresis was observed in loading and unloading of the equilibrium shear stress behavior. When axial compressive strain was applied it was observed that the values of G' and G" attained from static and dynamic oscillatory shear experiments increased. This trend was also observed in the equilibrium shear stress as well as stiffening of the hysteresis loop. Application of constant shear strain revealed the rupture point of the cornea when loaded with varying strain rates as the shear stress-strain behavior stiffened with increasing strain rate.

6.2 Future research

Preliminary studies were conducted to determine the effects of proteoglycans on corneal mechanics however these experiments were not conclusive thus additional work is required to quantify the possible contributions of proteoglycans on corneal mechanics. In the preliminary work, healthy corneas, and proteoglycan depleted corneas were tested in unconfined compression similar to techniques used in chapter 3. Proteoglycan depleted corneas were attained by incubating healthy porcine corneas in 0.1 U/ml of chondroitinase ABC enzyme in a reaction buffer at 37°C for two different time period; this was done to determine the effects of incubation time on the amount of proteoglycan depleted[147, 159].

The amount of proteoglycans depleted from enzymatic digestion was assessed in a qualitative and quantities manner. Qualitative analysis was conducted by histological analysis where sections of fresh and proteoglycan depleted corneas were fixed in formalin[160, 161], sliced and stained with toluidine blue dye[162]. Toluidine blue dye reacts with sulfated proteoglycans to produce purple coloration, thus proteoglycan depleted corneas would display lower purple intensity in comparison to fresh corneas when observed with a microscope. Quantitative analysis was conducted by attaining a standard curve of chondroitin sulfate C and toluidine blue at different concentrations[163]. Cyclohexane was used to breakdown the chondroitin sulfate complex, the mixture was separated and its intensity measured using a spectrometer thus attaining a standard curve. Healthy and proteoglycan depleted corneas were hydrated in OBSS and the washings of OBSS attained from these groups of corneas were mixed with toluidine blue, after which their intensities were measured. The measured intensity was converted to chondroitin sulfate concentration based on the standard curve.

Quantitative and qualitative analysis displayed the reduction of proteoglycans with incubation time and the addition of chondroitinase ABC enzyme, however the reaction buffer was also observed to have an effect on the amount of proteoglycans depleted. Changes in mechanical behavior were observed with incubation time and the addition of chondroitinase ABC enzyme however the effect of incubation time was also observed to affect its mechanical behavior thus a conclusion on the effect of proteoglycans on corneal mechanics could not be solely determined.

Possible suggestions to advance this pilot study could include the use of higher concentration of chondroitinase ABC enzyme in order to reduce the incubation time, addition of Dulbecco PBS at the end of enzymatic digestion for rinsing purposes[164] in order to attain higher levels of proteoglycan depletion. In addition, Papain[165-167] could also be used to determine the amount of proteoglycans in the cornea instead of the amounts of proteoglycans extruded from the cornea.

In the current study, results attained from static and dynamic oscillatory shear stresses, shear stress relaxation and shear viscometry were not modeled, furthermore these results highlights the notion of intrinsic viscoelasticity especially for experiments conducted at small amplitude shear strain where the flow of fluid does not affect the viscoelastic behavior of the cornea. This indicated the need for the addition of intrinsic viscoelasticity to the flow dependent viscoelasticity displayed by the transversely isotropic biphasic model.

The dynamic shear properties attained in this study were confined to the limits of linear viscoelasticity while in real world shear stresses applied to the cornea could exceed this limit thus large amplitude oscillatory shear studies need to be conducted to characterize dynamic response of the cornea to large strains.

REFERENCES

1. Petsche SJ, Chernyak D, Martiz J, Levenston ME, Pinsky PM. Depth-dependent transverse shear properties of the human corneal stroma. *Investigative ophthalmology & visual science* 2012;53:873-880.

2. Grierson I. *The Eye Book: Eyes and Eye Problems Explained*: Liverpool University Press; 2000.

3. Oyster CW. *The Human Eye: Structure And Function*: Sinauer Associates; 1999.

4. Ratner BD, Hoffman AS, Schoen FJ, Lemons JE. *Biomaterials Science: An Introduction to Materials in Medicine*: Elsevier Science; 2012.

5. Whitcher JP, Srinivasan M, Upadhyay MP. Corneal blindness: a global perspective. *Bulletin-Whorld Health organization* 2001;79:214-221.

6. Kinsey VE, Cogan DG. The Cornea: iii. Hydration Properties of Excised Corneal Pieces. *Archives of Ophthalmology* 1942;28:272-284.

7. Duane TD. The steady state of corneal hydration. *American journal of ophthalmology* 1949;32 Pt. 2:203-207.

8. Maurice DM. The structure and transparency of the cornea. *The Journal of physiology* 1957;136:263.

9. Ytteborg J, Dohlman CH. Corneal edema and intraocular pressure. II. Clinical results. *Arch Ophthalmol* 1965;74:477-484.

10. Nyquist GW. Rheology of the cornea: experimental techniques and results. *Exp Eye Res* 1968;7:183-188.

11. Anseth A. Studies on corneal polysaccharides. V. Changes in corneal glycosaminoglycans in transient stromal edema. *Exp Eye Res* 1969;8:297-301.

12. Hodson S. Why the cornea swells. *Journal of theoretical biology* 1971;33:419-427.

13. Andreassen TT, Hjorth Simonsen A, Oxlund H. Biomechanical properties of keratoconus and normal corneas. *Experimental Eye Research* 1980;31:435-441.

14. Patel S, Alió JL, Javaloy J, Perez-Santonja JJ, Artola A, Rodriguez-Prats J. Human Cornea Before and After Refractive Surgery Using a New Device: VCH-1. *Cornea* 2008;27:1042-1049 1010.1097/ICO.1040b1013e318172fc318140.

15. Scerrati E. Laser in situ keratomileusis vs. laser epithelial keratomileusis (LASIK vs. LASEK). *Journal of refractive surgery (Thorofare, NJ : 1995)* 2001;17:S219-221.

16. Wang H, Prendiville PL, McDonnell PJ, Chang WV. An ultrasonic technique for the measurement of the elastic moduli of human cornea. *Journal of biomechanics* 1996;29:1633-1636.

17. Orwin EJ, Borene ML, Hubel A. Biomechanical and Optical Characteristics of a Corneal Stromal Equivalent. *Journal of Biomechanical Engineering* 2003;125:439-444.

18. Borene ML, Barocas VH, Hubel A. Mechanical and cellular changes during compaction of a collagen-sponge-based corneal stromal equivalent. *Annals of biomedical engineering* 2004;32:274-283.

19. McPhee TJ, Bourne WM, Brubaker RF. Location of the stress-bearing layers of the cornea. *Investigative Ophthalmology & Visual Science* 1985;26:869-872.

20. Kasprzak HT, Robert Iskander D. Approximating ocular surfaces by generalised conic curves. *Ophthalmic & physiological optics : the journal of the British College of Ophthalmic Opticians (Optometrists)* 2006;26:602-609.

21. Faber C, Scherfig E, Prause JU, Sorensen KE. Corneal thickness in pigs measured by ultrasound pachymetry in vivo. *Scand J Lab Anim Sci* 2008;35:39-43.

22. Sanchez I, Martin R, Ussa F, Fernandez-Bueno I. The parameters of the porcine eyeball. *Graefe's Archive for Clinical and Experimental Ophthalmology* 2011;249:475-482.

23. Doughty MJ, Jonuscheit S. An assessment of regional differences in corneal thickness in normal human eyes, using the Orbscan II or ultrasound pachymetry. *Optometry (St Louis, Mo)* 2007;78:181-190.

24. Doughty MJ, Zaman ML. Human corneal thickness and its impact on intraocular pressure measures: a review and meta-analysis approach. *Survey of ophthalmology* 2000;44:367-408.

25. Doughty MJ, Petrou S, Macmillan H. Anatomy and morphology of the cornea of bovine eyes from a slaughterhouse. *Canadian journal of zoology* 1995;73:2159-2165.

26. Chan T, Payor S, Holden BA. Corneal thickness profiles in rabbits using an ultrasonic pachometer. *Investigative Ophthalmology & Visual Science* 1983;24:1408-1410.

27. Bozkir G, Bozkir M, Dogan H, Aycan K, Guler B. Measurements of axial length and radius of corneal curvature in the rabbit eye. *Acta medica Okayama* 1997;51:9-11.

28. Lee D-H, Kim D-H, Park S-H. Age and Sex Related Changes in Corneal Thickness and Anterior Corneal Curvature in Korean Young Population with Orbscan II Topography System. *Journal of the Optical Society of Korea* 2011;15:68-73.

29. Hogan MJ, Alvarado JA, Weddell JE. *Histology of the human eye: an atlas and textbook [by] Michael J. Hogan, Jorge A. Alvarado [and] Joan Esperson Weddell*: Saunders; 1971.

30. Hoeltzel DA, Altman P, Buzard K, Choe K-i. Strip Extensiometry for Comparison of the Mechanical Response of Bovine, Rabbit, and Human Corneas. *Journal of Biomechanical Engineering* 1992;114:202-215.

31. Hedbys BO, Mishima S, Maurice DM. The imbibition pressure of the corneal stroma. *Experimental Eye Research* 1963;2:99-IN91.

32. Komai Y, Ushiki T. The three-dimensional organization of collagen fibrils in the human cornea and sclera. *Investigative Ophthalmology & Visual Science* 1991;32:2244-2258.

33. Merindano Encina MD, Potau J, Ruano D, Costa J, Canals M. A comparative study of Bowman's layer in some mammals: Relationships with other constituent corneal structures. *European Journal of anatomy* 2002;6:133-140.

34. Ehlers N, Hjortdal J. The Cornea: Epithelium and Stroma. In: Fischbarg J (ed), *Advances in Organ Biology*: Elsevier; 2005:83-111.

35. Elsheikh A, Alhasso D, Rama P. Assessment of the epithelium's contribution to corneal biomechanics. *Exp Eye Res* 2008;86:445-451.

36. Hassell JR, Kimura JH, Hascall VC. Proteoglycan Core Protein Families. *Annual Review of Biochemistry* 1986;55:539-567.

37. Fatt I. *Physiology of the eye: an introduction to the vegetative functions*: Butterworths; 1978.

38. Dohlman CH. The function of the corneal epithelium in health and disease. The Jonas S. Friedenwald Memorial Lecture. *Investigative ophthalmology* 1971;10:383-407.

39. Last JA, Liliensiek SJ, Nealey PF, Murphy CJ. Determining the mechanical properties of human corneal basement membranes with atomic force microscopy. *J Struct Biol* 2009;167:19-24.

40. Jue B, Maurice DM. The mechanical properties of the rabbit and human cornea. *Journal of Biomechanics* 1986;19:847-853.

41. Hayashi S, Osawa T, Tohyama K. Comparative observations on corneas, with special reference to bowman's layer and descemet's membrane in mammals and amphibians. *Journal of Morphology* 2002;254:247-258.

42. Marshall GE, Konstas AG, Lee WR. Immunogold fine structural localization of extracellular matrix components in aged human cornea. II. Collagen types V and VI. *Graefe's archive for clinical and experimental ophthalmology = Albrecht von Graefes Archiv fur klinische und experimentelle Ophthalmologie* 1991;229:164-171.

43. Konomi H, Hayashi T, Nakayasu K, Arima M. Localization of type V collagen and type IV collagen in human cornea, lung, and skin. Immunohistochemical evidence by anti-collagen antibodies characterized by immunoelectroblotting. *The American journal of pathology* 1984;116:417-426.

44. Newsome DA, Foidart JM, Hassell JR, Krachmer JH, Rodrigues MM, Katz SI. Detection of specific collagen types in normal and keratoconus corneas. *Invest Ophthalmol Vis Sci* 1981;20:738-750.

45. Nakayasu K, Tanaka M, Konomi H, Hayashi T. Distribution of types I, II, III, IV and V collagen in normal and keratoconus corneas. *Ophthalmic research* 1986;18:1-10.

46. Hedbys BO, Dohlman CH. A new method for the determination of the swelling pressure of the corneal stroma in vitro. *Experimental Eye Research* 1963;2:122-129.

47. Lee D, Wilson G. Non-uniform swelling properties of the corneal stroma. *Current eye research* 1981;1:457-461.

48. Hodson SA. Corneal stromal swelling. *Progress in Retinal and Eye Research* 1997;16:99-116.

49. Almubrad T, Akhtar S. Structure of corneal layers, collagen fibrils, and proteoglycans of tree shrew cornea. *Molecular vision* 2011;17:2283-2291.

50. Johnson Dh BWMCR. The ultrastructure of descemet's membrane: I. changes with age in normal corneas. *Archives of Ophthalmology* 1982;100:1942-1947.

51. Jakus MA. Studies on the Cornea. II. The Fine Structure of Descement's Membrane. *The Journal of Biophysical and Biochemical Cytology* 1956;2:243-252.

52. Marshall GE, Konstas AG, Lee WR. Immunogold fine structural localization of extracellular matrix components in aged human cornea. I. Types I-IV collagen and laminin. *Graefe's archive for clinical and experimental ophthalmology = Albrecht von Graefes Archiv fur klinische und experimentelle Ophthalmologie* 1991;229:157-163.

53. Yokoi T, Seko Y, Yokoi T, et al. Establishment of Functioning Human Corneal Endothelial Cell Line with High Growth Potential. *PLoS ONE* 2012;7:e29677.

54. Li LY, Tighe BJ, Ruberti JW. Mathematical modelling of corneal swelling. *Biomech Model Mechanobiol* 2004;3:114-123.

55. Fischbarg J, Maurice DM. An update on corneal hydration control. *Experimental Eye Research* 2004;78:537-541.

56. Rajendra AU, Eddie NYk, Jasjit SS. *Image Modeling of the Human Eye* Norwood: Artech House; 2008.

57. Thiagarajah JR, Verkman AS. Aquaporin Deletion in Mice Reduces Corneal Water Permeability and Delays Restoration of Transparency after Swelling. *Journal of Biological Chemistry* 2002;277:19139-19144.

58. Olsen T, Sperling S. The swelling pressure of the human corneal stroma as determined by a new method. *Experimental Eye Research* 1987;44:481-490.

59. Hodson S, O'Leary D, Watkins S. The measurement of ox corneal swelling pressure by osmometry. *The Journal of physiology* 1991;434:399-408.

60. Brightbill FS, McGhee CNJ, McDonnell PJ. *Corneal Surgery: Theory, Technique and Tissue*: Mosby; 2009.

61. Smolin G, Foster CS, Azar DT, Dohlman CH. *Smolin and Thoft's The Cornea: Scientific Foundations and Clinical Practice*: Lippincott Williams & Wilkins; 2005.

62. Maurice DM. *The Eye: The Cornea and Sclera*. 3 ed. New York: Academic Press; 1984.

63. Meek KM, Leonard DW. Ultrastructure of the corneal stroma: a comparative study. *Biophysical Journal* 1993;64:273-280.

64. Elsheikh A, Brown M, Alhasso D, Rama P, Campanelli M, Garway-Heath D. Experimental assessment of corneal anisotropy. *Journal of refractive surgery (Thorofare, NJ : 1995)* 2008;24:178-187.

65. Elsheikh A, Alhasso D. Mechanical anisotropy of porcine cornea and correlation with stromal microstructure. *Experimental Eye Research* 2009;88:1084-1091.

66. Boote C, Dennis S, Huang Y, Quantock AJ, Meek KM. Lamellar orientation in human cornea in relation to mechanical properties. *Journal of Structural Biology* 2005;149:1-6.

67. Meyer K, Linker A, Davidson EA, Weissmann B. The mucopolysaccharides of bovine cornea. *The Journal of biological chemistry* 1953;205:611-616.

68. Michelacci YM. Collagens and proteoglycans of the corneal extracellular matrix. *Brazilian journal of medical and biological research = Revista brasileira de pesquisas medicas e biologicas / Sociedade Brasileira de Biofisica [et al]* 2003;36:1037-1046.

69. Hassell JR, Cintron C, Kublin C, Newsome DA. Proteoglycan changes during restoration of transparency in corneal scars. *Archives of Biochemistry and Biophysics* 1983;222:362-369.

70. Cintron C, Hassinger LC, Kublin CL, Cannon DJ. Biochemical and ultrastructural changes in collagen during corneal wound healing. *Journal of ultrastructure research* 1978;65:13-22.

71. Holmes DF, Gilpin CJ, Baldock C, Ziese U, Koster AJ, Kadler KE. Corneal collagen fibril structure in three dimensions: Structural insights into fibril assembly, mechanical properties, and tissue organization. *Proceedings of the National Academy of Sciences* 2001;98:7307-7312.

72. Gyi TJ, Meek KM, Elliott GF. Collagen interfibrillar distances in corneal stroma using synchrotron X-ray diffraction: a species study. *International Journal of Biological Macromolecules* 1988;10:265-269.

73. Hayes S, Boote C, Lewis J, et al. Comparative Study of Fibrillar Collagen Arrangement in the Corneas of Primates and Other Mammals. *The Anatomical Record: Advances in Integrative Anatomy and Evolutionary Biology* 2007;290:1542-1550.

74. Hedbys BO. The role of polysaccharides in corneal swelling. *Experimental Eye Research* 1961;1:81-91.

75. Meek KM, Fullwood NJ, Cooke PH, et al. Synchrotron x-ray diffraction studies of the cornea, with implications for stromal hydration. *Biophysical Journal* 1991;60:467-474.

76. Huang YF, Meek KM, Wang LQ, Wang DJ. Effects of prior freezing or drying on the swelling behaviour of the bovine cornea. *Chinese medical journal* 2009;122:212-218.

77. Davidson EA, Meyer K. Chondroitin, a new mucopolysaccharide. *The Journal of biological chemistry* 1954;211:605-611.

78. Chakravarti S, Magnuson T, Lass JH, Jepsen KJ, LaMantia C, Carroll H. Lumican regulates collagen fibril assembly: skin fragility and corneal opacity in the absence of lumican. *The Journal of cell biology* 1998;141:1277-1286.

79. Castoro JA, Bettelheim AA, Bettelheim FA. Water gradients across bovine cornea. *Invest Ophthalmol Vis Sci* 1988;29:963-968.

80. Scott JE, Bosworth TR. The comparative chemical morphology of the mammalian cornea. *Basic and applied histochemistry* 1990;34:35-42.

81. Parfitt GJ, Pinali C, Akama TO, et al. Electron tomography reveals multiple self-association of chondroitin sulphate/dermatan sulphate proteoglycans in Chst5-null mouse corneas. *Journal of Structural Biology* 2011;174:536-541.

82. Wilson SE, Kim WJ. Keratocyte apoptosis: implications on corneal wound healing, tissue organization, and disease. *Invest Ophthalmol Vis Sci* 1998;39:220-226.

83. Wilson SE, He YG, Weng J, et al. Epithelial injury induces keratocyte apoptosis: hypothesized role for the interleukin-1 system in the modulation of corneal tissue organization and wound healing. *Exp Eye Res* 1996;62:325-327.

84. West-Mays JA, Dwivedi DJ. The keratocyte: corneal stromal cell with variable repair phenotypes. *The international journal of biochemistry & cell biology* 2006;38:1625-1631.

85. Dohlman CH, Hedbys BO, Mishima S. The Swelling Pressure of the Corneal Stroma. *Investigative Ophthalmology & Visual Science* 1962;1:158-162.

86. Woo SLY, Kobayashi AS, Schlegel WA, Lawrence C. Nonlinear material properties of intact cornea and sclera. *Experimental Eye Research* 1972;14:29-39.

87. Tolpin DW, Klyce SD, Dohlman CH. Swelling properties of dogfish cornea. *Experimental Eye Research* 1969;8:429-437.

88. Friedmann MH, Kearns JP, Michenfelder CJ, Green K. Contribution of the Donnan osmotic pressure to the swelling pressure of corneal stroma. *The American journal of physiology* 1972;222:1565-1570.

89. Hart RW, Farrell RA. Structural theory of the swelling pressure of corneal stroma in saline. *Bulletin of Mathematical Biophysics* 1971;33:165-186.

90. Fatt I. The coefficient of thermal expansion of stroma. *Experimental Eye Research* 1971;12:254-260.

91. Wiley T, Fatt I. Effects of solutes on the swelling pressure of the corneal stroma. *Investigative ophthalmology* 1975;14:684-688.

92. Hodson S, Wigham C, Williams L, Mayes KR, Graham MV. Observation on the human cornea in vitro. *Exp Eye Res* 1981;32:353-360.

93. Dohlman CH, Anseth A. The swelling pressure of the ox corneal stroma. *Acta ophthalmologica* 1957;35:73-84.

94. Friedman MH, Green K. Swelling rate of corneal stroma. *Experimental Eye Research* 1971;12:239-250.

95. Eisenberg SR, Grodzinsky AJ. The kinetics of chemically induced nonequilibrium swelling of articular cartilage and corneal stroma. *Journal of biomechanical engineering* 1987;109:79.

96. Eisenberg SR, Grodzinsky AJ. Swelling of articular cartilage and other connective tissues: electromechanochemical forces. *Journal of orthopaedic research* 1985;3:148-159.

97. Kim W, Argento A, Rozsa FW, Mallett K. Constitutive behavior of ocular tissues over a range of strain rates. *J Biomech Eng* 2012;134:061002.

98. Elsheikh A, Kassem W, Jones SW. Strain-rate sensitivity of porcine and ovine corneas. *Acta of bioengineering and biomechanics / Wroclaw University of Technology* 2011;13:25-36.

99. Wollensak G, Spoerl E, Seiler T. Stress-strain measurements of human and porcine corneas after riboflavin–ultraviolet-A-induced cross-linking. *Journal of Cataract & Refractive Surgery* 2003;29:1780-1785.

100. Boyce BL, Jones RE, Nguyen TD, Grazier JM. Stress-controlled viscoelastic tensile response of bovine cornea. *Journal of Biomechanics* 2007;40:2367-2376.

101. Elsheikh A, Alhasso D, Rama P. Biomechanical properties of human and porcine corneas. *Experimental Eye Research* 2008;86:783-790.

102. Zeng Y, Yang J, Huang K, Lee Z, Lee X. A comparison of biomechanical properties between human and porcine cornea. *Journal of Biomechanics* 2001;34:533-537.

103. Boschetti F, Triacca V, Spinelli L, Pandolfi A. Mechanical Characterization of Porcine Corneas. *Journal of Biomechanical Engineering* 2012;134:031003-031009.

104. Elsheikh A, Wang D, Pye D. Determination of the modulus of elasticity of the human cornea. *Journal of Refractive Surgery* 2007;23:808-818.

105. Bryant MR, McDonnell PJ. Constitutive Laws for Biomechanical Modeling of Refractive Surgery. *Journal of Biomechanical Engineering* 1996;118:473-481.

106. Boyce BL, Grazier JM, Jones RE, Nguyen TD. Full-field deformation of bovine cornea under constrained inflation conditions. *Biomaterials* 2008;29:3896-3904.

107. Hjortdal JO. Extensibility of the normo-hydrated human cornea. *Acta ophthalmologica Scandinavica* 1995;73:12-17.

108. Hjortdal JO, Jensen PK. In vitro measurement of corneal strain, thickness, and curvature using digital image processing. *Acta ophthalmologica Scandinavica* 1995;73:5-11.

109. Kling S, Remon L, Pérez-Escudero A, Merayo-Lloves J, Marcos S. Corneal Biomechanical Changes after Collagen Cross-Linking from Porcine Eye Inflation Experiments. *Investigative Ophthalmology & Visual Science* 2010;51:3961-3968.

110. Mattson MS, Huynh J, Wiseman M, Coassin M, Kornfield JA, Schwartz DM. An in vitro intact globe expansion method for evaluation of cross-linking treatments. *Invest Ophthalmol Vis Sci* 2010;51:3120-3128.

111. Lombardo M, Lombardo G, Carbone G, De Santo MP, Barberi R, Serrao S. Biomechanics of the anterior human corneal tissue investigated with atomic force microscopy. *Invest Ophthalmol Vis Sci* 2012;53:1050-1057.

112. Last JA, Thomasy SM, Croasdale CR, Russell P, Murphy CJ. Compliance profile of the human cornea as measured by atomic force microscopy. *Micron (Oxford, England : 1993)* 2012;43:1293-1298.

113. Winkler M, Chai D, Kriling S, et al. Nonlinear Optical Macroscopic Assessment of 3-D Corneal Collagen Organization and Axial Biomechanics. *Investigative Ophthalmology & Visual Science* 2011;52:8818-8827.

114. Soergel F, Jean B, Seiler T, et al. Dynamic mechanical spectroscopy of the cornea for measurement of its viscoelastic properties in vitro. *German journal of ophthalmology* 1995;4:151-156.

115. Nickerson CS. Engineering the mechanical properties of ocular tissues. California Institute of Technology; 2006.

116. Elliott GF, Goodfellow JM, Woolgar AE. Swelling studies of bovine corneal stroma without bounding membranes. *The Journal of Physiology* 1980;298:453-470.

117. Cheng X, Hatami-Marbini H, Pinsky P. Modeling Collagen-Proteoglycan Structural Interactions in the Human Cornea. In: Holzapfel GA, Kuhl E (eds), *Computer Models in Biomechanics*: Springer Netherlands; 2013:11-24.

118. Mow VC, Kuei SC, Lai WM, Armstrong CG. Biphasic Creep and Stress Relaxation of Articular Cartilage in Compression: Theory and Experiments. *Journal of Biomechanical Engineering* 1980;102:73-84.

119. Armstrong CG, Lai WM, Mow VC. An analysis of the unconfined compression of articular cartilage. *Journal of biomechanical engineering* 1984;106:165-173.

120. Soltz MA, Ateshian GA. Experimental verification and theoretical prediction of cartilage interstitial fluid pressurization at an impermeable contact interface in confined compression. *Journal of biomechanics* 1998;31:927-934.

121. Cohen B, Lai WM, Mow VC. A transversely isotropic biphasic model for unconfined compression of growth plate and chondroepiphysis. *Journal of biomechanical engineering* 1998;120:491-496.

122. Soltz MA, Ateshian GA. A Conewise Linear Elasticity Mixture Model for the Analysis of Tension-Compression Nonlinearity in Articular Cartilage. *Journal of Biomechanical Engineering* 2000;122:576-586.

123. Huang C-Y, Mow VC, Ateshian GA. The Role of Flow-Independent Viscoelasticity in the Biphasic Tensile and Compressive Responses of Articular Cartilage. *Journal of Biomechanical Engineering* 2001;123:410-417.

124. Lau W, Pye D. Changes in Corneal Biomechanics and Applanation Tonometry with Induced Corneal Swelling. *Investigative Ophthalmology & Visual Science* 2011;52:3207-3214.

125. Li L, Pinsky PM. A nonlinear macroscopic multi-phasic model for describing interactions between solid, fluid and ionic species in biological tissue materials. *Philosophical Magazine* 2011;91:300-314.

126. Studer HP, Riedwyl H, Amstutz CA, Hanson JVM, Büchler P. Patient-specific finite-element simulation of the human cornea: A clinical validation study on cataract surgery. *Journal of biomechanics* 2013;46:751-758.

127. Jayasuriya AC, Scheinbeim JI, Lubkin V, Bennett G, Kramer P. Piezoelectric and mechanical properties in bovine cornea. *Journal of biomedical materials research Part A* 2003;66:260-265.

128. Ahearne M, Yang Y, Then KY, Liu KK. An indentation technique to characterize the mechanical and viscoelastic properties of human and porcine corneas. *Annals of biomedical engineering* 2007;35:1608-1616.

129. Mortazavi AM, Simon BR, Stamer WD, Vande Geest JP. Drained secant modulus for human and porcine peripapillary sclera using unconfined compression testing. *Experimental Eye Research* 2009;89:892-897.

130. Cheng S, Bilston LE. Unconfined compression of white matter. *Journal of Biomechanics* 2007;40:117-124.

131. Huang C-Y, Stankiewicz A, Ateshian GA, Mow VC. Anisotropy, inhomogeneity, and tension–compression nonlinearity of human glenohumeral cartilage in finite deformation. *Journal of biomechanics* 2005;38:799-809.

132. Huang C-Y, Soltz MA, Kopacz M, Mow VC, Ateshian GA. Experimental Verification of the Roles of Intrinsic Matrix Viscoelasticity and Tension-Compression Nonlinearity in the Biphasic Response of Cartilage. *Journal of Biomechanical Engineering* 2003;125:84-93.

133. Doughty MJ. Swelling of the collagen-keratocyte matrix of the bovine corneal stroma ex vivo in various solutions and its relationship to tissue thickness. *Tissue & cell* 2000;32:478-493.

134. Kim JH, Green K, Martinez M, Paton D. Solute permeability of the corneal endothelium and Descemet's membrane. *Experimental Eye Research* 1971;12:231-238.

135. Fullwood NJ, Meek KM. An ultrastructural, time-resolved study of freezing in the corneal stroma. *Journal of molecular biology* 1994;236:749-758.

136. Broadwater JJ, Schorling JJ, Herring IP, Elvinger F. Effect of body position on intraocular pressure in dogs without glaucoma. *American Journal of Veterinary Research* 2008;69:527-530.

137. Linder BJ, Trick GL, Wolf ML. Altering body position affects intraocular pressure and visual function. *Investigative ophthalmology & visual science* 1988;29:1492-1497.

138. Hara T, Maurice DM. Changes in the swelling pressure of the corneal stroma with time, hydration and temperature, determined by a new method. *Exp Eye Res* 1972;14:40-48.

139. DiSilvestro MR, Zhu Q, Suh J-KF. Biphasic Poroviscoelastic Simulation of the Unconfined Compression of Articular Cartilage: II---Effect of Variable Strain Rates. *Journal of Biomechanical Engineering* 2001;123:198-200.

140. June RK, Fyhrie DP. A comparison of cartilage stress-relaxation models in unconfined compression: QLV and stretched exponential in combination with fluid flow. *Computer methods in biomechanics and biomedical engineering* 2011.

141. Elsheikh A, Wang D, Kotecha A, Brown M, Garway-Heath D. Evaluation of Goldmann Applanation Tonometry Using a Nonlinear Finite Element Ocular Model. *Annals of biomedical engineering* 2006;34:1628-1640.

142. Martinez-de-la-Casa JM, Garcia-Feijoo J, Fernandez-Vidal A, Mendez-Hernandez C, Garcia-Sanchez J. Ocular Response Analyzer versus Goldmann Applanation Tonometry for Intraocular Pressure Measurements. *Investigative Ophthalmology & Visual Science* 2006;47:4410-4414.

143. Asejczyk-Widlicka M, Śródka W, Schachar RA, Pierścionek BK. Material properties of the cornea and sclera: A modelling approach to test experimental analysis. *Journal of Biomechanics* 2011;44:543-546.

144. Pandolfi A, Manganiello F. A model for the human cornea: constitutive formulation and numerical analysis. *Biomech Model Mechanobiol* 2006;5:237-246.

145. Kampmeier J, Radt B, Birngruber R, Brinkmann R. Thermal and Biomechanical Parameters of Porcine Cornea. *Cornea* 2000;19:355-363.

146. Hedbys BO, Mishima S. Flow of water in the corneal stroma. *Experimental Eye Research* 1962;1:262-275.

147. Hedbys BO. Corneal resistance of the flow of water after enzymatic digestion. *Exp Eye Res* 1963;2:112-121.

148. Stewart JM, Schultz DS, Lee O-T, Trinidad ML. Collagen Cross-Links Reduce Corneal Permeability. *Investigative Ophthalmology & Visual Science* 2009;50:1606-1612.

149. Horlocker TT, Wedel DJ. Density, specific gravity, and baricity of spinal anesthetic solutions at body temperature. *Anesthesia and analgesia* 1993;76:1015-1018.

150. de Freitas Fonseca M, Andrade CM, Jr., de Mello MJ, Crispi CP. Effect of temperature on fluidity of irrigation fluids. *British journal of anaesthesia* 2011;106:51-56.

151. Edwards A, Prausnitz MR. Fiber matrix model of sclera and corneal stroma for drug delivery to the eye. *AIChE Journal* 1998;44:214-225.

152. Maas SA, Ateshian GA, Weiss JA, Ellis BJ. FEBio: Finite Elements for Biomechanics. *Journal of Biomechanical Engineering* 2012;134:011005-011005.

153. Gao L-L, Zhang C-Q, Dong L-M, Jia Y-W. Description of depth-dependent nonlinear viscoelastic behavior for articular cartilage in unconfined compression. *Materials Science and Engineering: C* 2012;32:119-125.

154. Pinsky PM, van der Heide D, Chernyak D. Computational modeling of mechanical anisotropy in the cornea and sclera. *Journal of cataract and refractive surgery* 2005;31:136-145.

155. Bilston LE, Liu Z, Phan-Thien N. Linear viscoelastic properties of bovine brain tissue in shear. *Biorheology* 1997;34:377-385.

156. Bilston LE, Liu Z, Phan-Thien N. Large strain behaviour of brain tissue in shear: some experimental data and differential constitutive model. *Biorheology* 2001;38:335-345.

157. Liu Z, Bilston LE. Large deformation shear properties of liver tissue. *Biorheology* 2002;39:735-742.

158. Shen F, Tay T, Li J, Nigen S, Lee P, Chan H. Modified Bilston nonlinear viscoelastic model for finite element head injury studies. *Journal of biomechanical engineering* 2006;128:797.

159. Yamagata T, Saito H, Habuchi O, Suzuki S. Purification and Properties of Bacterial Chondroitinases and Chondrosulfatases. *Journal of Biological Chemistry* 1968;243:1523-1535.

160. Stix B, Leber M, Bingemer P, et al. Hereditary Lattice Corneal Dystrophy Is Associated with Corneal Amyloid Deposits Enclosing C-Terminal Fragments of Keratoepithelin. *Investigative Ophthalmology & Visual Science* 2005;46:1133-1139.

161. Tamaki K, Yamaguchi T, Varnell E, Kaufman H. Histological study of corneas preserved in two new media. *British journal of ophthalmology* 1987;71:570-577.

162. Alomar TS, Al-Aqaba M, Gray T, Lowe J, Dua HS. Histological and Confocal Microscopy Changes in Chronic Corneal Edema: Implications for Endothelial Transplantation. *Investigative Ophthalmology & Visual Science* 2011;52:8193-8207.

163. Tillman J, Ullm A, Madihally SV. Three-dimensional cell colonization in a sulfate rich environment. *Biomaterials* 2006;27:5618-5626.

164. Fishbein KW, Canuto HC, Bajaj P, Camacho NP, Spencer RG. Optimal methods for the preservation of cartilage samples in MRI and correlative biochemical studies. *Magnetic resonance in medicine : official journal of the Society of Magnetic Resonance in Medicine / Society of Magnetic Resonance in Medicine* 2007;57:866-873.

165. Wight TN, Kinsella MG, Keating A, Singer JW. Proteoglycans in human long-term bone marrow cultures: biochemical and ultrastructural analyses. *Blood* 1986;67:1333-1343.

166. Nakazawa K, Hassell JR, Hascall VC, Newsome DA. Heterogeneity of proteoglycans in monkey corneal stroma. *Archives of biochemistry and biophysics* 1983;222:105-116.

167. Nakazawa K, Newsome DA, Nilsson B, Hascall VC, Hassell JR. Purification of keratan sulfate proteoglycan from monkey cornea. *The Journal of biological chemistry* 1983;258:6051-6055.

VITA

Ebitimitula Etebu

Candidate for the Degree of

Master of Science

Thesis: MECHANICAL AND RHEOLOGICAL CHARACTERIZATION OF THE CORNEA
Major Field: Mechanical Engineering

Biographical:

Education:

Completed the requirements for the Master of Science/Arts in your major at Oklahoma State University, Stillwater, Oklahoma in December, 2013.

Completed the requirements for the Bachelor of Science/Arts in your major at Oklahoma State University, Stillwater, Oklahoma in 2010.

Experience:

Research Assistant. Computational Mechanics Lab. Stillwater, Ok.

- Develop mechanical testing protocols used to performed static or dynamic mechanical tests. Analyzed the stress relaxation and strain rate dependent behavior of viscoelastic materials.
- Created anisotropic-hyperelastic and viscoelastic finite element models for fibrous composites based on composite microstructure using COMSOL multiphysics and other FEA packages
- Provide 3D CAD design, design optimization, parts vendor communications, and bill of materials for the design and build of laboratory devices

Teaching Assistant. Department of Mechanical and Aerospace engineering, O.S.U Stillwater, Ok.

- Assisted Professor with the grading, and supervision of an undergraduate mechanical design course.
- Assisted students with problem solving by explaining /clarifying linear elastic deformation theorems, stress analysis and failure theorems taught in the course

Design Project. Goodyear Tire & Rubber Company, Lawton, OK

- Worked with research and development to design and optimize a web-handling process used to convert wasted web materials into wound webs useful materials for downstream processing
- Implemented a web-handling process that unwinds, guides, slitters, and winds wasted web materials.

Professional Memberships: Student Member; ASME, AAPG.